AD-A090 585 SOUTHERN METHODIST UNIV DALLAS TX DEPT OF CIVIL AND --ETC F/G 20/4
MEASUREMENTS OF UNSTEADY TURBULENT BOUNDARY LAYERS WITH PRESSUR--ETC(U)
AUG 80 R L SIMPSON, Y CHEW, B G SHIVAPRASAD DAAG29-76-G-0187
UNCLASSIFIED WT-6 ARO-13367.4-EX NL

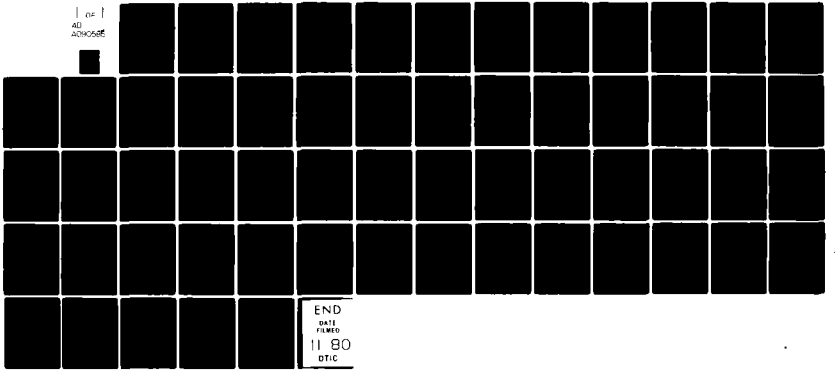

(12)

MEASUREMENTS OF UNSTEADY TURBULENT BOUNDARY LAYERS WITH PRESSURE GRADIENTS

FINAL REPORT

R. L. Simpson, Y.-T. Chew, and B. G. Shivaprasad

August 1980

U.S. Army Research Office

Grant DAAG29-76-G-0187

Southern Methodist University
Department of Civil and Mechanical Engineering

Report WT-6

THE VIEW, OPINIONS, AND/OR FINDINGS CONTAINED IN THIS REPORT ARE THOSE OF THE AUTHORS AND SHOULD NOT BE CONSTRUED AS AN OFFICIAL DEPARTMENT OF *THE ARMY POSITION, POLICY, OR DECISION, UNLESS SO DESIGNATED BY OTHER* DOCUMENTATION.

Unclassified

SECURITY CLASSIFICATION OF THIS PAGE (When Data Entered)

REPORT DOCUMENTATION PAGE		READ INSTRUCTIONS BEFORE COMPLETING FORM
1. REPORT NUMBER	2. GOVT ACCESSION NO. AD-A090 585	3. RECIPIENT'S CATALOG NUMBER
4. TITLE (and Subtitle) MEASUREMENTS OF UNSTEADY TURBULENT BOUNDARY LAYERS WITH PRESSURE GRADIENTS		5. TYPE OF REPORT & PERIOD COVERED (9) Final Report 1 April 1976 - 31 May 1979
		6. PERFORMING ORG. REPORT NUMBER WT-6
7. AUTHOR(s) (10) R. L. Simpson, Y.-T. Chew, and B. G. Shivaprasad		8. CONTRACT OR GRANT NUMBER(s) (15) DAAG29-76-G-0187
9. PERFORMING ORGANIZATION NAME AND ADDRESS		10. PROGRAM ELEMENT, PROJECT, TASK AREA & WORK UNIT NUMBERS
11. CONTROLLING OFFICE NAME AND ADDRESS U. S. Army Research Office Post Office Box 12211 Research Triangle Park, NC 27709		12. REPORT DATE (11) August 1980
		13. NUMBER OF PAGES
14. MONITORING AGENCY NAME & ADDRESS (if different from Controlling Office)		15. SECURITY CLASS. (of this report) Unclassified
		15a. DECLASSIFICATION/DOWNGRADING SCHEDULE

16. DISTRIBUTION STATEMENT (of this Report)

[illegible] A

17. DISTRIBUTION STATEMENT (of the abstract entered in Block 20, if different from Report)

NA

18. SUPPLEMENTARY NOTES

The view, opinions, and/or findings contained in this report are those of the author(s) and should not be construed as an official department of the Army position, policy, or decision unless so designated by other documentation.

19. KEY WORDS (Continue on reverse side if necessary and identify by block number)

Turbulence
Unsteady Flow
Boundary Layer
Separation
Pressure Gradients
Laser Anemometry

20. ABSTRACT (Continue on reverse side if necessary and identify by block number)

Although periodic unsteady turbulent boundary layers are of real significance in turbomachines and helocopters, little experimental velocity distribution data have been obtained, especially with flow separation. An unsteady turbulent boundary layer facility was developed at SMU to produce almost-sinusoidal waveforms for practical reduced frequencies of the order of unity. Separation occurred on the flat test-wall of the diverging test

DD FORM 1 JAN 73 1473 EDITION OF 1 NOV 65 IS OBSOLETE

SECURITY CLASSIFICATION OF THIS PAGE (When Data Entered)

(20) section. An active boundary layer control system was developed to prevent separation on non-test walls of the test section.

Detailed measurements using laser and hot-wire anemometry were made at reduced frequencies of 0.55 and 1.0. Well upstream of separation the flow away from the wall behaved in a quasi-steady manner. Near the wall an unexpected phase shift occurs, which is incompletely explained and may be an instrumentation and apparatus dependent effect.

Near separation and downstream, more interaction of the periodic and turbulent motions occurs since the characteristic large eddy bursting frequency decreases with length along the flow. The flow near the wall in the separated region has a substantial phase lead over the outer region flow. While U, U^2, v^2, and $-uv$ are nearly in phase well upstream of separation, in the separation zone U and $-\overline{uv}$ are nearly in phase with $\overline{u^2}$ and $\overline{v^2}$ having a large phase lag.

TABLE OF CONTENTS

APPENDICES

LIST OF FIGURES

NOMENCLATURE

C	length of converging-diverging portion of test section
$C_f/2$	$\equiv \tau_w/\rho U_\infty^2$, local skin-friction coefficient
$\overline{f}$	time mean value of f and F
$\tilde{f}$	organized periodic part of f and F
f	$\equiv$ turbulent fluctuation of f
f	$\equiv \overline{f} + \tilde{f} + f$, instantaneous signal
F	$\equiv \overline{f} + \tilde{f}$, ensemble-average of f for a specific phase
k	thermal conductivity
k	$\equiv \omega C/2\overline{U}_{\infty e}$, reduced frequency
k	von Karman constant in eqn. (1.6)
L	characteristic large length scale
N	distance from the wall to the minimum velocity in the backflow
P	pressure
Re_c	$\equiv \overline{U}_{\infty e} C/\nu$, Reynolds number
T	period of imposed oscillation
t	time

U, V, W	ensemble-averaged velocities in x, y, z directions, respectively
u, v, w	turbulent fluctuation velocities in x, y, z directions, respectively
$\overline{u^2}, \overline{v^2}, \overline{w^2}$	ensemble-averaged values of u^2, v^2, and w^2
u', v', w'	rms values of $\overline{u^2}$, $\overline{v^2}$, and $\overline{w^2}$
$\overline{-uv}$	ensemble-averaged Reynolds shear stress
U_τ	$\equiv (\tau_w/\rho)^{\frac{1}{2}}$, shear velocity
U^+	$\equiv U/U_\tau$
$\overline{U}_{\infty e}$	mean test section entrance velocity
x, y, z	streamwise, normal, and spanwise coordinates

Greek Symbols

δ	y where $U = 0.99\ U_\infty$
ϕ_n	phase angle of n^{th} harmonic
ν	kinematic viscosity
ρ	density
τ	shearing stress

Subscripts

E, ∞	freestream or condition outside shear flow

n	harmonic number, e.g., 1, 2, etc.
w	denotes wall value

I. INTRODUCTION

I.A Importance of Unsteady Turbulent Boundary Layers

Unsteady turbulent boundary layers have become the subject of much recent interest because of unsteady aerodynamic phenomena associated with blades in compressors and turbines and with helicopter rotors in translating motion. While all turbulent flows are inherently unsteady, the term "unsteady" will mean here an organized time dependent motion, in contrast to the relatively unorganized motion of turbulence. The boundary layers cannot be ignored in unsteady flow analyses because there is considerable interaction between the boundary layer and the inviscid flow during high lift operating conditions of these devices. In such cases the relatively thick boundary layer on the suction side of the lifting body is near separation.

In spite of its importance, relatively little fundamental work oriented toward describing the behavior of unsteady turbulent boundary layers has been done. Very little of this work has been done on unsteady turbulent boundary layers near separation. Interest in this subject was revived in the early 1970's, when several steady flow turbulent boundary layer prediction procedures were extended to the unsteady case. The only experimental data that were available at the time were those of Karlsson (1959) for zero-mean-pressure-gradient cases. Although Karlsson had indicated that non-linear interaction effects produced by moderately large fluctuation amplitudes were small, agreement with prediction methods that included this assumption was still not very satisfactory. Unacceptable disagreement also existed among various theoretical methods (Telionis, 1977).

Consequently, in the mid-1970's several experimental programs, including the one at SMU, were begun to provide a data base for prediction modeling of unsteady turbulent boundary layers.

As pointed out below, few measurements have been made of the viscous sublayer of an unsteady turbulent boundary layer. Measurements of the viscous sublayer are included here, with unexpected behavior.

I.B Previous Work on Unsteady Turbulent Boundary Layers

Unsteady turbulent boundary layers are governed by the same equations as for the steady case, except that time-dependent effects must be included. The continuity and momentum equations for incompressible unsteady turbulent boundary layers are, respectively:

$$\frac{\partial U}{\partial x} + \frac{\partial V}{\partial y} = 0 \tag{1.1}$$

and

$$\frac{\partial U}{\partial t} + U\frac{\partial U}{\partial x} + V\frac{\partial U}{\partial y} = \frac{\partial U_e}{\partial t} + U_e\frac{\partial U_e}{\partial x} + \frac{\partial}{\partial y}\left[\nu \frac{\partial U}{\partial y} - \overline{uv}\right] \tag{1.2}$$

Here U and V are ensemble-averaged streamwise and normal-to-wall velocity components and $\overline{-uv}$ is the ensemble-averaged Reynolds shear stress.

For periodic unsteady flow, the ensemble average of instantaneous values of a quantity F for a specific phase $(2\pi t/T)$ of the outer flow oscillation is given by

$$F = \lim_{N\to\infty} \frac{1}{N} \sum_{N=0}^{N} F(t + NT) \tag{1.3}$$

where T is the period of the imposed oscillation and N is the number of cycles that are averaged. This ensemble average is also called a "periodic sample" or a "phase average." F can also be represented as

$$F = \overline{f} + \tilde{f} + f \tag{1.4}$$

where $\overline{f}$ is the time-averaged or mean value, $\tilde{f}$ is the organized fluctuation, and f is the turbulent fluctuation. By comparison of these two equations

$$F = \overline{f} + \tilde{f}. \tag{1.5}$$

The difficulty of solving equations (1.1) and (1.2) is the same as that for steady flows, namely, describing the behavior of $\overline{-uv}$. A number of investigators have argued that as long as the period of the organized unsteadiness is relatively long as compared to the turbulence time scales, it should be acceptable to use the approximation that the turbulence structure is unaffected by the unsteadiness. When the frequency of the organized unsteadiness is comparable to energy-containing turbulence frequencies or the "bursting" frequency, this approximation cannot be used. Substantial interaction between the organized and unorganized time-dependent motions would be expected. For example, Acharya and Reynolds (1975) have shown that several turbulence models fail for the latter condition in an unseparated channel flow.

Bradshaw (1978) pointed out that the substantial derivative of $\overline{-uv}$, $D(\overline{-uv})/ Dt$, for the ensemble-averaged movement of a fluid element cannot exceed values for which the turbulence model is satisfactory in steady flow and still be valid in unsteady flow. Separate bounds on the streamwise wavelength and on frequency in a spatially-dependent unsteady flow are not required; the upper limit on the frequency seen by a moving fluid element can be derived from steady-flow considerations. If a steady flow turbulence model cannot respond to spatial changes with a wavelength less than L, then the moving-axis frequency of the unsteady flow cannot exceed U_E / L.

Nearly all of the experimental data that have been obtained have been outside the viscous sublayer and near wall region. Patel (1977) measured U and $\overline{u^2}$ in travelling wave zero-pressure-gradient flows for oscillation

amplitudes up to 11% of the mean freestream velocity and 4-12 Hz. Kenison (1977) obtained the same type of measurements and Preston tube skin friction results in the same tunnel with a mean adverse pressure gradient. The O.N.E.R.A. group (Houdeville et al., 1976; Cousteix et al., 1977, 1979) have obtained U, $\overline{u^2}$, $\overline{-uv}$, $\overline{v^2}$, and kurtosis measurements for zero-mean-pressure-gradient and adverse-pressure-gradient-time-dependent flows. The oscillation frequency was between 38 to 43 Hz with the oscillation amplitudes of 0.1 to 0.37 of the mean freestream velocity. All of these measurements indicate that outside the near wall region the turbulence structure is basically unaffected by organized unsteadiness. While the validity of the steady flow Preston tube skin friction technique for unsteady flow appears logical in view of the above-mentioned work, the measurements presented here indicate that the steady flow law of the wall may not hold for the viscous sublayer of unsteady flows. Thus the basis for the Preston tube technique in unsteady flow is still in question.

In their unseparated channel flow, Acharya and Reynolds (1975) measured a substantial phase lead for the sublayer oscillation over the core flow velocity in their 24Hz experiment. A substantial phase lag was observed in the sublayer for a frequency of 40Hz, which was the bursting frequency for the steady flow with the same mean velocity. Karlsson (1959) also reported a phase shift of as much as 35° in the viscous sublayer, but he did not have enough data to isolate the effect. Here we present data for the viscous sublayer. None of the current prediction methods can account for substantial phase variations within the viscous sublayer.

Two analytical investigations suggest that a "critical layer," where the velocity of wave propagation of disturbances equals the flow velocity, may exist near the wall in which the organized unsteady and turbulent motions can

interact. Benney and Lin (1960) examined the effect of a time-periodic oscillation on a viscous flow with a spanwise-periodic velocity variation. Since steady turbulent boundary layers have some spanwise dependent motion and a "critical layer," their problem may be thought of as an idealized counterpart for the near wall region of an unsteady turbulent boundary layer. They found that non-linear terms of the order of the square of the oscillation amplitude produce non-linear effects near the critical layer that are larger than the square of the oscillation amplitude. The streamwise vortical secondary motion remains large even outside the critical layer.

In the second investigation, Davis (1974) used a dynamical model to predict perturbation turbulent Reynolds stresses. He assumed that an infinitesimal perturbation results in a linear change in the statistics of the turbulence and that the turbulence is either weak or that the turbulent perturbations are quasi-Gaussian. He applied this to long-wave perturbations, finding that the perturbation shear stress is of primary dynamical importance and is determined by the spectrum of $\overline{v^2}$ and the perturbation velocity of $\tilde{U}$. Large shear values for a given spectral frequency occur at its critical height. After summing this interaction between the periodic and all turbulent motions, he obtained the result

$$\tilde{\tau} = 2k\ (\overline{-uv})^{\frac{1}{2}}\ y\ \frac{d\tilde{U}}{dy} \qquad (1.6)$$

for the perturbation shear stress outside the viscous sublayer. As shown in later discussion, this equation is equivalent to the mixing length theory result.

I.C Objectives of Current Work

The original objectives of the current work were to obtain experimental data for several moderately large amplitude oscillatory unsteady turbulent

boundary layers that separated. As described in the next chapter, considerable experimental apparatus and instrumentation development was required to enable the acquisition of high quality data. In view of the previous research, it was expected that most of the phenomena of interest in practical flows could be handled by steady turbulence models, although an insufficient data base was available to confirm this assumption. Consequently, it was somewhat surprising to find substantial interaction between the periodic flow and the turbulence in the separating and separated flow region. Detailed laser and hot-wire anemometer measurements in the separating flow region are presented here.

No previous unsteady turbulent boundary layer study has reported viscous sublayer measurements that confirm the quasi-steady model for low reduced frequencies. It was surprising to find apparently anomalous hot-wire anemometer measurements in the viscous sublayer. Later, the papers by Benney and Lin and by Davis were discovered, which at least support the possibility that this sublayer behavior may be real rather than an apparatus and instrumentation induced anomaly.

In order to measure the surface shearing stress, a Rubesin et al. (1975) type of surface hot-wire gage with a low thermal conductivity subrate was developed. No previous direct measurements of the surface shearing stress have been made.

As a result of these observations, considerably more time and effort were spent on repeating measurements than originally planned. Thus, results for only two reduced frequencies were obtained. However, it is clear that previously unreported effects exist in the viscous sublayer and in the separated flow region. This final report summarizes the results of this research.

II. EXPERIMENTAL EQUIPMENT

II.A Basic Wind Tunnel

As shown schematically in Fig. 1 the mainstream flow of the blown open-circuit wind tunnel is introduced into the test section after first passing through a filter, blower, a fixed-setting damper, a plenum, a section of honeycomb to remove the mean swirl of the flow, seven screens to remove much of the turbulence intensity, and finally through a two-dimensional 4:1 contraction ratio nozzle to further reduce the longitudinal turbulence intensity while accelerating the flow to test speed. These same components were in an earlier version of this wind tunnel with a shorter test section that was used in previous research (Simpson et al., 1977; Simpson and Wallace, 1975; Simpson and Shackleton, 1977). The rotating-blade damper, which produced the flow unsteadiness, is described in section II.B below.

Fig. 2 is a side view schematic of the 8 m long, 0.91 m wide test section of the wind tunnel. The upper wall is adjustable such that the free-stream velocity or pressure gradient can be adjusted. The side walls are made of float plate glass to prevent laser signal dispersion while the upper wall is made of plexiglass.

The test wall is constructed from 19 mm thick fin-form plywood, reinforced every 28 cm with 7.6 x 3.8 x 0.6 cm cross section steel channel. This reinforcement was necessary since Acharya and Reynolds (1975) found that test wall vibration amplitudes as small as 0.025 mm produced up to a 10% error in $\tilde{U}$ measurements near the wall. They reduced their vibrations by adding a large amount of mass to the test wall. In the present case the entire weight of the test section rests on the test wall and the steel reinforcements.

The active boundary layer control system, which is described in section

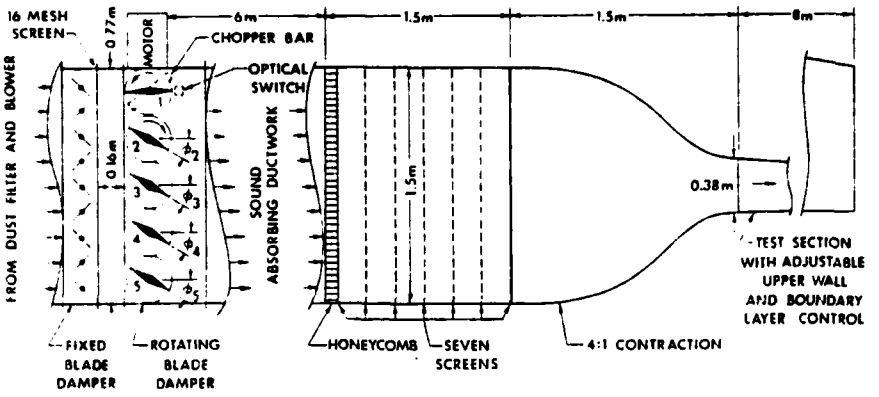

Figure 1. Schematic of the SMU Wind Tunnel (Simpson et al., 1978).

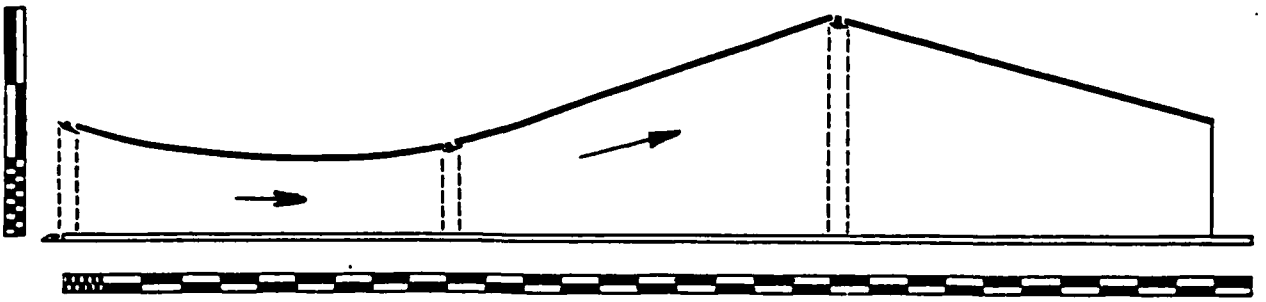

Figure 2. Sideview schematic of the test section. Major divisions on scales: 10 inches. Note baffle plate upstream of blunt leading edge on bottom test wall and side and upper wall jet boundary layer controls.

II.C below, is used to eliminate preferential separation of the curved top wall boundary layer. Highly two-dimensional wall jets of high velocity air are introduced at the beginning of each of the eight feet long sections. At the latter two streamwise locations the oncoming boundary layer is partially removed by a highly two-dimensional suction system.

The inviscid core flow is uniform within 0.05% in the spanwise direction and within 1% in the vertical direction with a turbulence intensity of 0.1% at 18 mps. The test wall boundary layer is tripped by the blunt leading edge of the plywood floor, the height of the step from the wind tunnel contraction to the test wall being 0.63 cm. Smoke can be introduced uniformly into the boundary layer just upstream of this trip for use with the laser anemometer.

II.B Programmable-Rotating-Blade Damper

Investigators of unsteady flows normally have little control over the waveform of the flow unsteadiness. Although the waveform may consist principally of a given frequency, substantial contributions normally come from higher harmonics. In anticipation of non-linear effects produced within an unsteady turbulent boundary layer, a programmable-rotating-blade damper and control system were designed, constructed, and used at SMU to produce a nearly single harmonic sinusoidal waveform without wind tunnel resonance. This feature allows one to attribute any large higher-harmonic effects within the boundary layer to boundary layer processes, rather than to combined effects with inviscid flow higher harmonics of the freestream.

Simpson et al. (1978) describe this rotating-blade-damper feedback control system in more detail. In essence, the angular velocity of the rotating blades in the damper is varied during a cycle so as to produce the desired waveform shape, amplitude, and frequency. In the current experiments,

the 0.596 Hz oscillation had a velocity amplitude that was one-third of the mean velocity. In these cases the amplitudes of the second and third harmonics were about 2 to 3% of the first harmonic. For comparison, it should be noted that for constant angular velocity blade rotation, the amplitude of the second harmonic is 14% of the first harmonic.

All events during an oscillation cycle were synchronized with respect to a "reference" square wave voltage signal at the oscillation frequency that is generated by the quartz clock in the control electronics. A "clock" square wave voltage signal with a frequency 96 times the reference signal is also generated to aid data acquisition.

The variation in the period of each flow cycle, or the "jitter," follows a Gaussian distribution with a standard deviation of 0.15%. This indicates a high degree of repeatability from cycle to cycle. Results obtained several weeks apart indicate long-term stability of the electronic system and long-term repeatability, which are important when performing experiments over a period of months.

II.C Boundary Layer Control System

An active boundary layer control system was installed on the non-test walls of the test section to inhibit undesirable flow three-dimensionality and to prevent separation. Because the static pressure in the test section is time varying in these experiments, no passive boundary layer control can be used that depends on a steady test section pressure higher than the pressure outside the tunnel. The active boundary layer control system removes low momentum fluid by sucking off the boundary layer and supplies high momentum fluid through tangential wall jets. Its performance is less influenced by the fluctuating test section static pressure than that of the previous passive system. The wall suction and wall jet units are located

at 2.54 m and 5.08 m on the non-test walls. Only the wall jet portion of this unit is installed at the test section entrance. Only the essential features of this system are summarized here; other details are contained in an unpublished report by Bowles (1977). All of the wall suction and wall jet units had identical cross sections. As much care as possible was taken to make these units geometrically and aerodynamically two-dimensional.

Two pressure taps were located in the nozzle of the jet and in the diffuser of the suction system. After calibration, the measured pressure difference between these taps allowed the nozzle and the diffuser to be used as jet flow and suction flow meters, respectively. Excellent linear calibrations were found between measured dynamic pressures and the respective differential pressures.

The average dynamic pressure of the jet exit flow was measured along the length of each unit with a 6.35 mm dia. impact probe. The standard deviation of the dynamic pressure variation was less than 2.5% along each of the jet units. The dynamic pressure in the 2 cm nearest the end of each unit was about 2/3 of that for the midsection. The jets at the test section entrance were operated at an average velocity of 27.4 mps; at the 2.54 m location the wall jet velocity was 36.6 mps for the upper wall and 22 mps for the side walls; at the 5.08 m location the upper wall and side wall jet velocities were 23 mps and 17.4 mps.

The variation of the dynamic pressure of the suction flow was measured along the length of each unit. The difference between the static pressure inside the diffuser at a particular location and atmospheric pressure had a standard deviation of no more than 2% along each suction unit. Most of the departure from uniformity occurred near the ends where, fortunately, about 20% greater suction dynamic pressure occurred. Thus a greater amount of

momentum deficient wind tunnel corner fluid could be removed, partly overcoming the effect of the dynamic pressure deficiency at the ends of the wall jet sections. The average suction velocity at the 2.54 m location was 13.7 mps while for the 5.08 m location it was 23 mps for the upper wall and 17 mps for the side walls.

The hot-wire anemometer mean velocity and streamwise turbulence intensity profiles in the midplane along the first streamwise upper wall suction unit were almost uniform. This indicates that some of the upstream flow is deflected toward the wall by the suction since the boundary layer velocity profile is not uniform. Immediately downstream the jet momentum is then rapidly mixed with the remaining upstream boundary layer flow.

It should be noted that the flows in this control system are relatively insensitive to the ± 1 cm of water static pressure oscillations in the test section. The large volume of the control system and the 30 cm of water static pressure loss in its components act as a large low pass frequency filter. Dynamic pressure oscillations of the wall jet flow were of the order ± 0.04 cm of water.

II.D Instrumentation

II.D.1. Hot-Wire Anemometers

Miller-type (1976) integrated circuit hot-wire anemometers and linearizers, as modified by Simpson et al. (1979) were constructed and used. A TSI Model 1050 anemometer was used with the surface hot-wire element that is described in section II.D.3 below. The frequency response was flat up to 7.5kHz for an overheat ratio of 0.7. This moderately high overheat ratio was used for two reasons. First, as shown by Wood (1975) the range of flat frequency response is improved with a higher overheat ratio. Secondly, a 0.2° C wind tunnel air temperature oscillation amplitude was present at the

flow oscillation frequency due to periodic dissipation and compressibility effects. In order to make this air temperature oscillation have a negligible effect on the hot-wire behavior, an overheat ratio as high as safely possible was desired. In the present case, this oscillation amplitude was only 0.04% of the temperature difference between the wire and the air, so no corrections to hot-wire measurements were made for this effect.

Standard TSI model 1274-TI.5 normal wire and model 1248-TI.5 cross-wire probes were used for boundary layer measurements. The closest to the wall that these probes could safely make measurements was about 0.05 mm and 0.9 mm, respectively. For the celerity measurements in the near wall region, a two sensor TSI model 1244-10 hot-film probe was used with 5.00 mm space between the parallel sensors. The sensing elements for the wire probes are 3.8 μm diameter, 1.27 mm sensing length platinum-plated tungsten wires while the elements for the hot-film probe are 0.025 mm diameter, 1 mm sensing length platinum-coated quartz rods.

The traversing mechanism used for the boundary layer velocity measurements was mounted on the supporting frame for the upper wall and provided for precise positioning of the probe sensors. A cathetometer was used to accurately locate the probe sensor from the wall within an uncertainty of about ± 0.002 inches. The detailed streamwise free-stream velocity distributions were obtained using the Model 1274-TI.5 probe mounted on a mobile cart.

A standard TSI model 1015 C correlator was used to obtain sum and difference values for u and v from cross-wire signals. When using the electronic multipliers to determine the turbulence quantities uv, u^2v, and v^3, each linearized hot-wire signal was passed first through a Q = 5 band-reject filter (Burr-Brown UAF41 Universal Filter) that was adjusted for

40dB attentuation at 0.596 Hz and for only 3dB attentuation at ± 10% on either side of this frequency. This eliminated the organized periodic fluctuation from the signals.

Lest there be any doubt regarding their performance, the Miller-type anemometers were found to produce faithful law-of-the-wall velocity profiles for a steady turbulent boundary layer (Simpson et al., 1980).

II.D.2 Laser Anemometer

The Laser anemometer used in these experiments is described in some detail by Simpson and Chew (1978). In essence this is a two-velocity-component (U,V) directionally-sensitive fringe type system that has been used in earlier work (Simpson et al., 1977). The particles follow the highly turbulent oscillations found in separated regions. Signal processing was by fast-sweep-rate sampling spectrum analysis, as described by Simpson and Barr (1975).

The LDV signal was treated the same as a continuous hot-wire signal, even though it is discontinuous. The LDV signal data rate must be sufficiently large that the latest signal processing output voltage is obtained since the sample for the last bin was taken. This insures that there is no more than one bin uncertainty in the phase information. Here the minimum data rate is 58 samples/sec, but since these new signals are not equally spaced in time, a higher data rate is necessary. About 400 new signals per second were obtained, which produced satisfactory U, $\overline{u^2}$, V and $\overline{v^2}$ results.

II.D.3 Surface Hot-Wire Skin Friction Element

It was pointed out in the Introduction that no previous studies of the viscous sublayer of unsteady turbulent boundary layers have been made. Consequently one cannot confidently use any method to determine the skin friction that assumes the validity of the law-of-the-wall velocity profile,

e.g., Preston tube or Clauser plot methods. The momentum integral equation method of determining the skin friction is relatively uncertain since the required streamwise derivatives in this equation are relatively uncertain to begin with. Hot-wire probes are known to interfere with the near wall flow (Oka and Kostic, 1972), so velocity gradients at the wall cannot be evaluated reliably. Thus a direct surface measurement is preferred.

The Rubesin et al. (1975) heat-transfer element is an attractive method of measuring the surface shearing stress because it is simple, compact, and easy and inexpensive to construct. It can be designed so that the same calibration curve is valid for both laminar and turbulent flow and is insensitive to pressure gradients, i.e., it is universally applicable. A standard constant-temperature hot-wire anemometer set, such as the TSI Model 1050 used here, can be used to power and control the element.

The principle underlying this skin-friction gage requires the surface-heating element to have a dimension in the streamwise direction that is small compared to the boundary-layer thickness. The thermal energy from the heated element, which is insulated from the surface sub-rate material, forms a thermal boundary layer within the viscous sublayer that is immediately adjacent to the surface. To maximize the element sensitivity to τ_w, a very low thermal conductivity k substrate must be used. Rubesin et al. used low impact grade polystyrene ($k = 0.0015$ W/cm^2) whereas Bellhouse and Schultz (1966) used quartz ($k = 0.011$ W/cm^2) and Liepmann and Skinner (1954) used ebonite ($k = 0.0078$ W/cm^2). High impact grade polystyrene has a much larger thermal conductivity. The ratio of the effective streamwise length to the actual gage length is much smaller, 2.5 as compared to 390 for the Liepmann and Skinner gage. The effective length needs to be as small as possible if pressure gradient and turbulent transport effects on the calibration can be

neglected. A smaller effective length makes the measured shear stress more sensitive to measured voltage changes. Rubesin et al., Murthy and Rose (1978), and Higuchi and Peake (1978) have shown that a polystyrene substrate gage has the same calibration in both laminar and turbulent flow that is independent of the pressure gradients.

A gage was constructed at SMU with the essential features of the Rubesin et al. gage. A 0.0025 cm diameter platinum - 10% rhodium wire was mounted between 1.32 mm diameter mickel electrodes located 1 cm apart whose ends were flush with the flat polystyrene surface. Conduction losses to the electrodes are small since the wire length to diameter ratio of 400 is large. Several drops of ethyl acetate were used to dissolve the polystyrene in the vicinity of the wire and imbed it in the surface. The ends of the wire were then soldered to the electrodes on the thin portable plexiglas plate on which the polystyrene was mounted. The resulting surface was sanded and polished flat and smooth before the wire was mounted. This plate allows a single element to be moved to various measurement locations with a minimum of flow disturbance.

Rubesin et al. found that overheat temperatures of at least 20° C were needed to make the heat loss from a wire proportional to its temperature rise. Peake and Higuchi found that overheats greater than 80° C caused the wire to melt the substrate and separate from the surface. Here the cold resistance at 25° C was 3.70 Ω and 0.5 Ω overheat resistance was used, so with a temperature coefficient of resistivity of $1.6 \times 10^{-3} C^{\circ -1}$ then ΔT was 84° C. The wire was not observed to separate from the surface.

A simple stainless steel cone with 0.5° angle between the cone and the plate surface was constructed for calibration of this gage. A brass housing held the cone in place on the plate. The hot-wire was aligned with a radial

line from the cone apex. The velocity gradient at the plate surface was independent of the radial position since the cone surface velocity and the spacing between the cone and the plate each vary linearly with the radius. A Miller-type exponential electronic linearizer was used to linearize the bride output signal. Results obtained for a steady turbulent boundary layer agreed with the Ludwig-Tillman (1950) skin friction equation (Simpson et al., 1980).

II.E Signal Processing

Ten channels of Line Driver Amplifiers link the Wind Tunnel Laboratory with the SMU Hybrid Computing Laboratory for data acquisition. The SMU Hybrid Computing Laboratory is equipped with an EAI 690 Hybrid Computer and support peripherals. The 690 system is composed of an EAI 680 general purpose analog computer, EAI 693 communication interface for analog to digital conversion, and an EAI 640 digital computer.

The EAI 640 is a general purpose minicomputer with a 32k core memory. The 640's peripherals include a Decwriter II terminal, cartridge tape unit, seven track mag tape, IBM 2481 and two IBM 2311 composing a disc system, high speed paper tape equipment, and a programmable internal timer. The 640 is also interfaced with the principal campus computer, a CDC Cyber 72.

In practice this system was operated in a real time data acquisition mode to determine ensemble-averaged velocities and turbulence fluctuations. The reference and clock square wave signals from the programmable rotating-blade-damper control system were used to trigger data acquisition. The negative-going slope of the reference signal marked the beginning of an oscillation cycle. The negative-going slope of the clock signal marked the acquisition of data for one of 96 different phases of the fundamental period. The Fortran program determined signal averages and variances for each of these 96 phases

for any number of oscillation cycles, which was 200 for all data presented here. These results were then temporarily stored and later transferred to the main campus computer, where data analysis, permanent storage on magnetic tape, and plotting of results took place.

A Princeton Applied Research Model 4512 Fast-Fourier Transform Spectrum Analyzer was used to determine the harmonic content of the organized periodic motion and the spectral content of the boundary layer turbulence. In the first application, it was used with the DC to 10 Hz range to verify that no extraneous periodic frequencies existed during an experiment and to aid the rapid initial adjustment of the programmable rotating-blade-damper control system in reducing all but the fundamental harmonic. In the measurement of turbulence spectra with the DC to 2kHz range, a phase-selector circuit, described below, was used to activate the acquisition of signals only during a selectable phase of the periodic cycle.

A phase selector circuit was constructed to produce a voltage pulse that activated the FFT only during a desired phase of a cycle. A Signetics 556 Dual Timer was trimmed such that a voltage pulse, 1/8 th of the reference signal period long, could be selected for one of 16 equally-spaced phases of a cycle. For example, with the selector-switch in the first position, the center of the 45° wide pulse was located at 22.5°.

Other electronic equipment included a SAICOR model 41 digital correlation and probability analyzer, an Applied University Research four-channel FM tape recorder (response down 3 db at 2 KHz), a voltage comparator or schmitt trigger using an operational amplifier integrated circuit and signal multipliers using Analog Devices AD533 JH integrated circuits trimmed to within ± 1% fullscale nonlinearity error. A true integrating voltmeter consisting of a voltage-controlled oscillator (Tektronix FG501 Function

Generator) and a digital counter (Tektronix DC503 Universal Counter) was used in checking the voltage signal mean values with the computer results.

III. DESCRIPTION OF TEST FLOWS

III.A Velocity Distributions

Two different oscillatory flows on the bottom wall of the test section shown in Fig. 2 were examined with the same periodic flow frequency, 0.596 Hz. The time-mean entrance velocity $\overline{U}_{\infty e}$ for flow A was 16.5 mps while it was 9.1 mps for flow B. Based upon these velocities and the 4.9 m length of the converging-diverging section for C, the length Reynolds numbers and reduced frequencies for thes flows are $\overline{U}_{\infty e}\, C/\nu = 5.1 \times 10^6$ and $\omega C/2\overline{U}_{\infty e} = 0.55$ for flow A and 2.9×10^6 and 1.00 for flow B. Fig. 3 shows the time-mean free-stream velocity distributions and envelopes of maximum and minimum velocities for these flows. The free-stream velocity distribution for a steady free-stream separating flow under separate study is also shown (Simpson et al., 1980). Note that the time-averaged freestream velocity distributions are nearly the same for the two cases except in the downstream region. The free-stream oscillation amplitude is about 1/3 of the time-mean. These non-dimensional conditions were selected since they are near the values encountered in some turbomachinery and helicopter applications. While these flows may be considered near quasi-steady, the moderate oscillation amplitude introduces some effects that are of interest, particularly in the separation region. All experimental data were obtained at an air temperature of 25 ± 1/4° C.

The ensemble-averaged freestream velocity outside of the boundary layer can be expressed in terms of its fourier components as

$$U_E = \overline{U}_E \left\{ 1 + \sum_{n=1}^{\infty} \left[\frac{U_{nE}}{\overline{U}_E} \cos\left(\omega n t - \phi_{nE} \right) \right] \right\} \qquad (3.1)$$

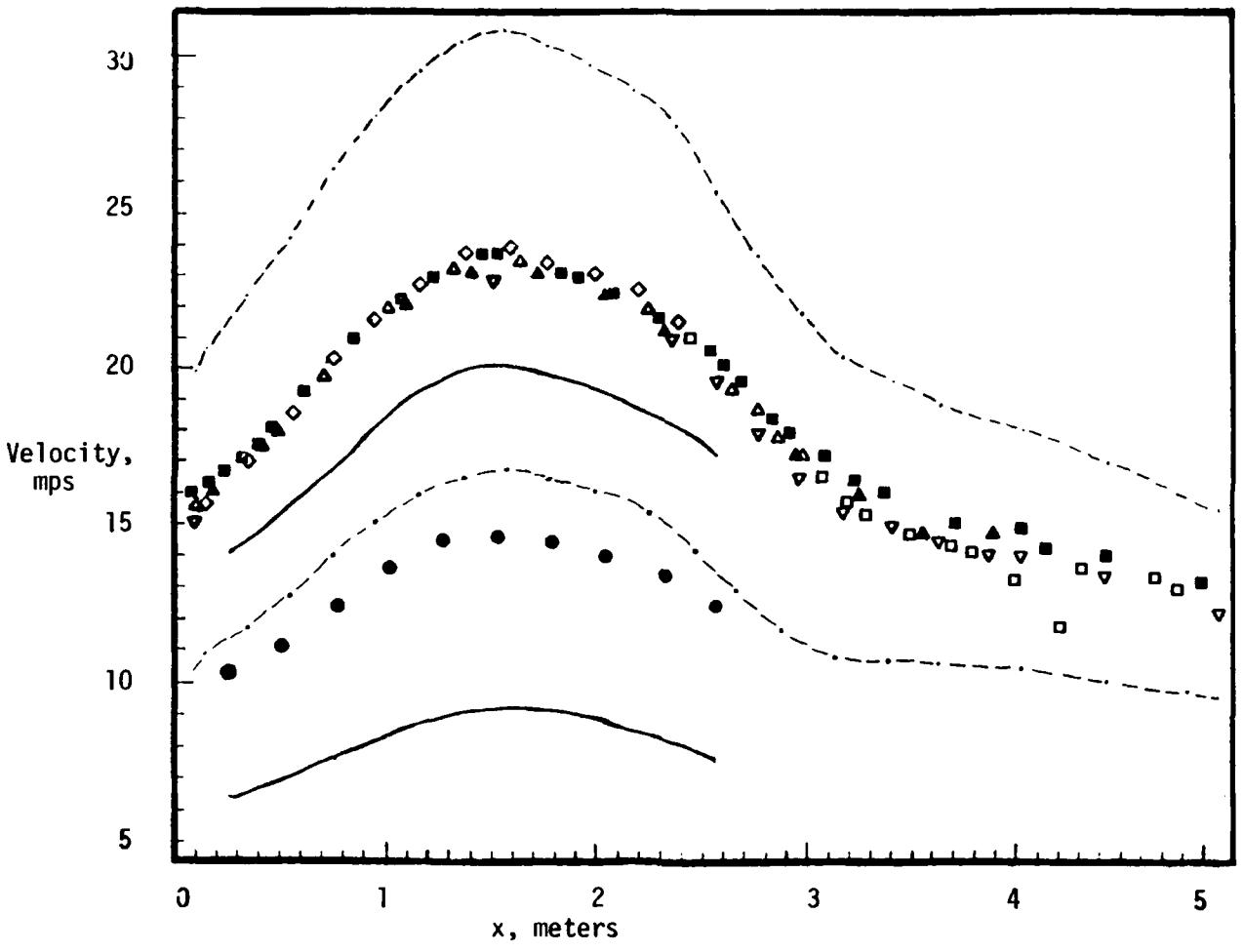

Figure 3. $\bar{U}_\infty$ with envelopes for oscillation amplitudes: —·— envelop for flow A; envelope for flow B ——— . Unsteady flow data: ◘ , 3/30/78; ◇ , 5/4/78; △ , 3/78; ▽ , 5/9/78; ▲ , 12//77, all for flow A. For flow B, ● . ■ Steady flow.

$\overline{U}_E$, U_{nE}, and ϕ_{nE} are in general functions of streamwise position and were highly repeatable during this research. Each set was obtained on a given day during a short period of time. Upstream of 3 m, $\overline{U}_E$ and $U_{1E}/\overline{U}_E$ repeat within 2% while ϕ_{1E} only varies 4 degrees.

Although the variable-angular-velocity rotating blade damper tended to eliminate higher harmonic effects, second and third harmonics had amplitudes about 2% of the first harmonic for flow A and about 3% for flow B. The scatter is about ± 15% for $U_{2E}/\overline{U}_E$ and only ± 5% for $U_{3E}/\overline{U}_E$ upstream of separation in flow A. Because of the relatively small contribution by these harmonics, relatively greater scatter in ϕ_{2E} and ϕ_{3E} occurs, ± 40° and ± 10°, respectively. Fast-fourier signal analysis revealed that only 0.298 Hz, which is the rotating damper blade frequency, and higher harmonics produce periodic velocity contributions.

The mean freestream streamwise turbulence intensity is within 1% upstream of separation. It is nearly independent of streamwise position, indicating no strong influence of flow acceleration or deceleration. Laser-illuminated smoke-flow visualization indicated no gross flow three-dimensionality upstream of separation while velocity profiles at several spanwise locations indicated that the mean velocity was two-dimensional within 1%. Downstream of 4.4 m no nominally two-dimensional flow remained.

III.B Pressure Gradient Distributions

The free-stream streamwise pressure gradient distribution for each flow was calculated from the measured free-stream velocity distributions, respectively, and the unsteady inviscid equation of motion

$$\frac{-1}{\rho}\frac{dP}{dx} = \frac{\partial U}{\partial t} + U\frac{\partial U}{\partial x} \qquad (3.2)$$

When eqn. (3.1) is substituted into eqn. (3.2) many sine and cosine terms with streamwise derivatives of all quantities result. Only the important terms were retained.

The first harmonic contributes a term of the order of about 1/2 $(U_{1E}/\overline{U}_E)^2$ times the mean velocity term to the mean pressure gradient because of the quadratic term in eqn. (3.2). Here the mean pressure gradient would be about 19/18 of that due to the mean velocity term alone upstream of separation. The minimum pressure gradient in flow A is about zero downstream in the separating flow region.

The first harmonic pressure gradient terms can be expressed as

$$\left[\overline{U}_E^2\,(U_{1E}'+U_{1E}U_E')^2 + U_{1E}^2\,(\overline{U}_E\phi_{1E}'-\omega)^2\right]^{1/2}\cos\,(\omega t-\phi_{1E}-180°-\gamma_{1E}) \qquad (3.3)$$

where

$$\gamma_{1E} = \arctan\,\frac{U_{1E}(\phi_{1E}'\,\overline{U}_E - \omega)}{\overline{U}_E\,U_{1E}' + U_{1E}\,\overline{U}_E'}$$

Figs. 4 and 5 show $(\phi_{1E} + 180° + \gamma_{1E})$ for flows A and B. As also shown in Figs. 4 and 5 the pressure gradient first harmonic strongly lags the local free-stream velocity in the converging section of the tunnel. The lag is considerably lower in the diverging section. After the beginning of separation the pressure gradient slightly leads the local free-stream velocity, as shown in Fig. 4.

IV. SUMMARY OF EXPERIMENTAL RESULTS

Ensemble-averaged values at each phase of the unsteadiness period for U, $\overline{u^2}$, $\overline{v^2}$, and $\overline{-uv}$ were obtained for a nearly pure sinusoidal velocity oscillation of 1/3 of the mean velocity at reduced frequencies of k = 0.55

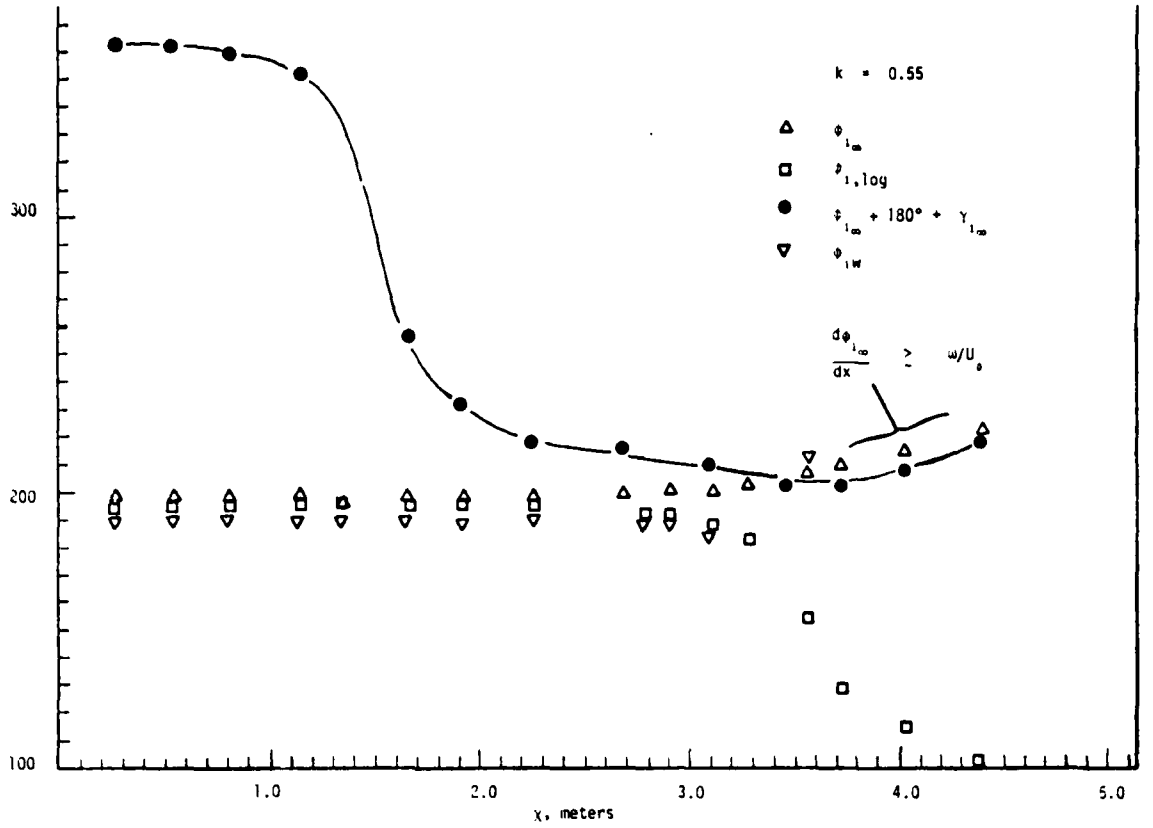

Figure 4. Phase angles of first harmonics for k = 0.55 flow: $\phi_{1\infty}$, free-stream velocity; $\phi_{1,log}$, logarithmic region velocity; pressure gradient, $\phi_{1\infty} + 180° + \gamma_{1\infty}$; wall shearing stress ϕ_{1W}.

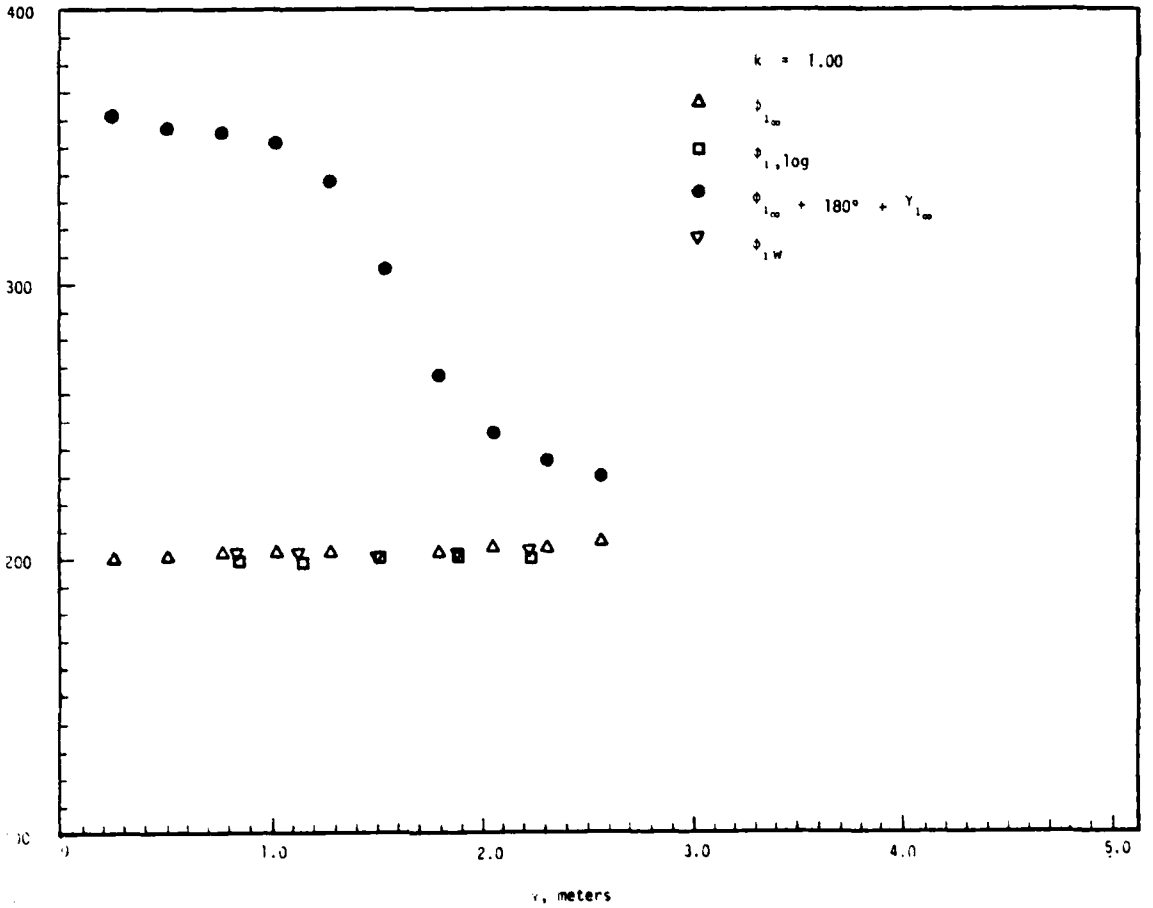

Figure 5. Phase angles of first harmonics for k = 1.00 flow: $\phi_{1\infty}$, free-stream velocity; $\phi_{1,log}$, logarithmic region velocity; pressure gradient, $\phi_{1\infty} + 180° + \gamma_{1\infty}$; wall shearing stress ϕ_{1W}.

and 1.00. The test flows were on the bottom wall of the converging-diverging-converging channel shown in Fig. 2. Only typical results are presented here for brevity. Complete data sets are on magnetic tape file with Dr. L. W. Carr* in the format used for the 1980-81 Stanford Conference on Complex Turbulent Flows. Eventually these data will be on file at Stanford University.**

Figures 6-13 show: (a) ensemble-averaged velocity waveforms at several y positions from the test wall; (b) ensemble-averaged velocity profiles at several phases of the oscillation period; (c) the phase angle of the first harmonic ϕ, as a function of position from the wall; and (d) the amplitude of the first two harmonics of the ensemble-averaged oscillation normalized on the local <u>average</u> velocity $\overline{U}$ as a function of position from the wall. Figures 14-17 show the phase angles for the first harmonic of U, $\overline{u^2}$, $\overline{v^2}$, and $\overline{-uv}$ all along flow A.

Well upstream of separation the flow in the outer region of the boundary layer is in phase. Outside the viscous dominated region, but closer to the wall than the logarithmic region, the ensemble-averaged unsteady oscillatory velocity leads the logarithmic region oscillatory velocity by as much as 60°. Spectral measurements in this region indicate that the turbulence frequencies vary drastically during the cycle period. Higher frequency turbulent oscillations are observed during the higher velocity part of the cycle while frequencies an order of magnitude lower are observed during the low velocity part. The oscillatory turbulent fluctuations are not in phase with the periodic ensemble-averaged U oscillations in this region.

* U.S. Army Aeromechanics Lab., NASA-Ames Research Center, Moffett Field, Ca. 94035.

** Contact Professor S. J. Kline, Thermosciences Division, Department of Mechanical Engineering, Stanford, Ca. 94305.

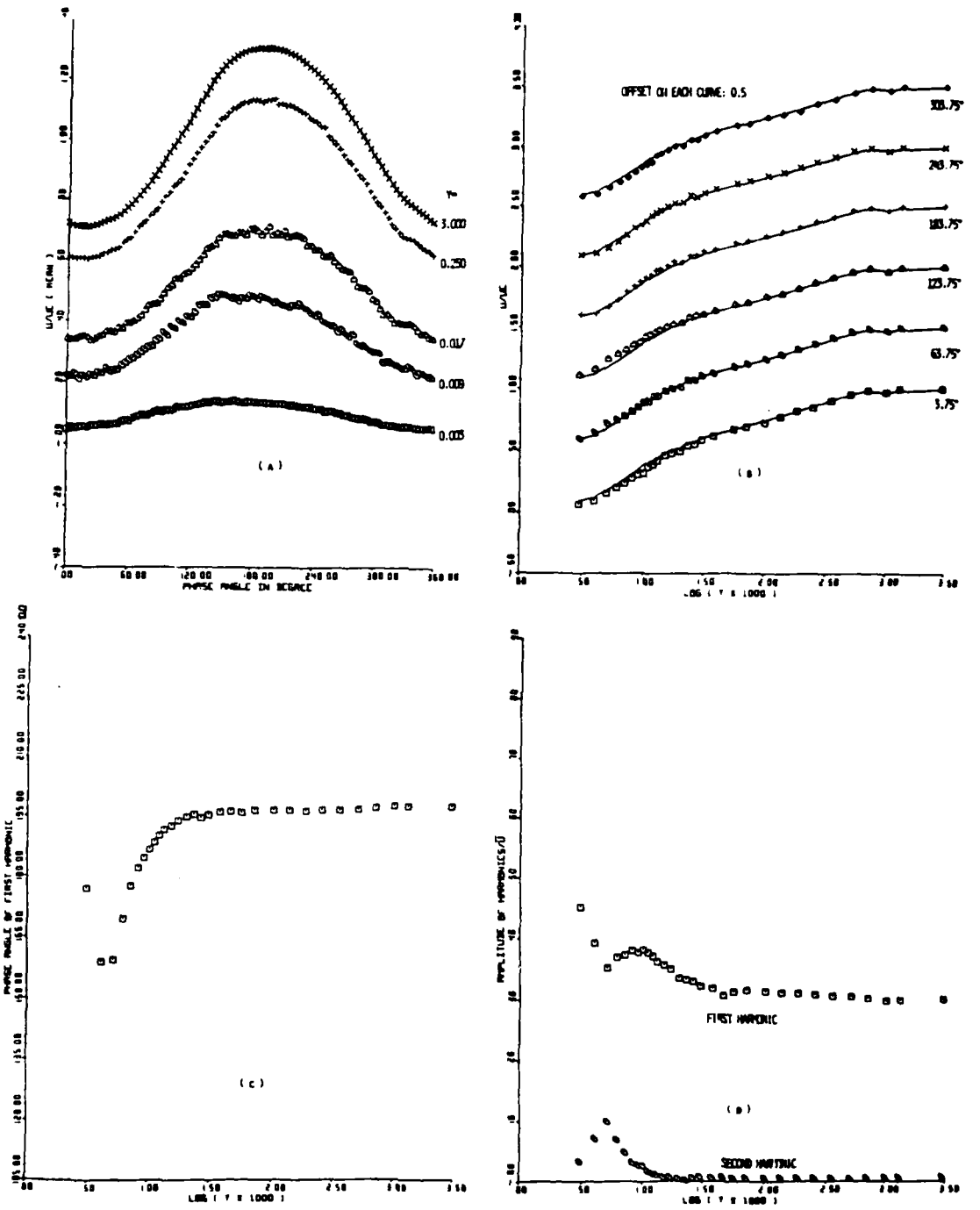

Figure 6. Flow A, ensemble-averaged normal hot-wire data, x= 44 3/4 inches. Y in inches, base-10 logs; phase angle in degrees.

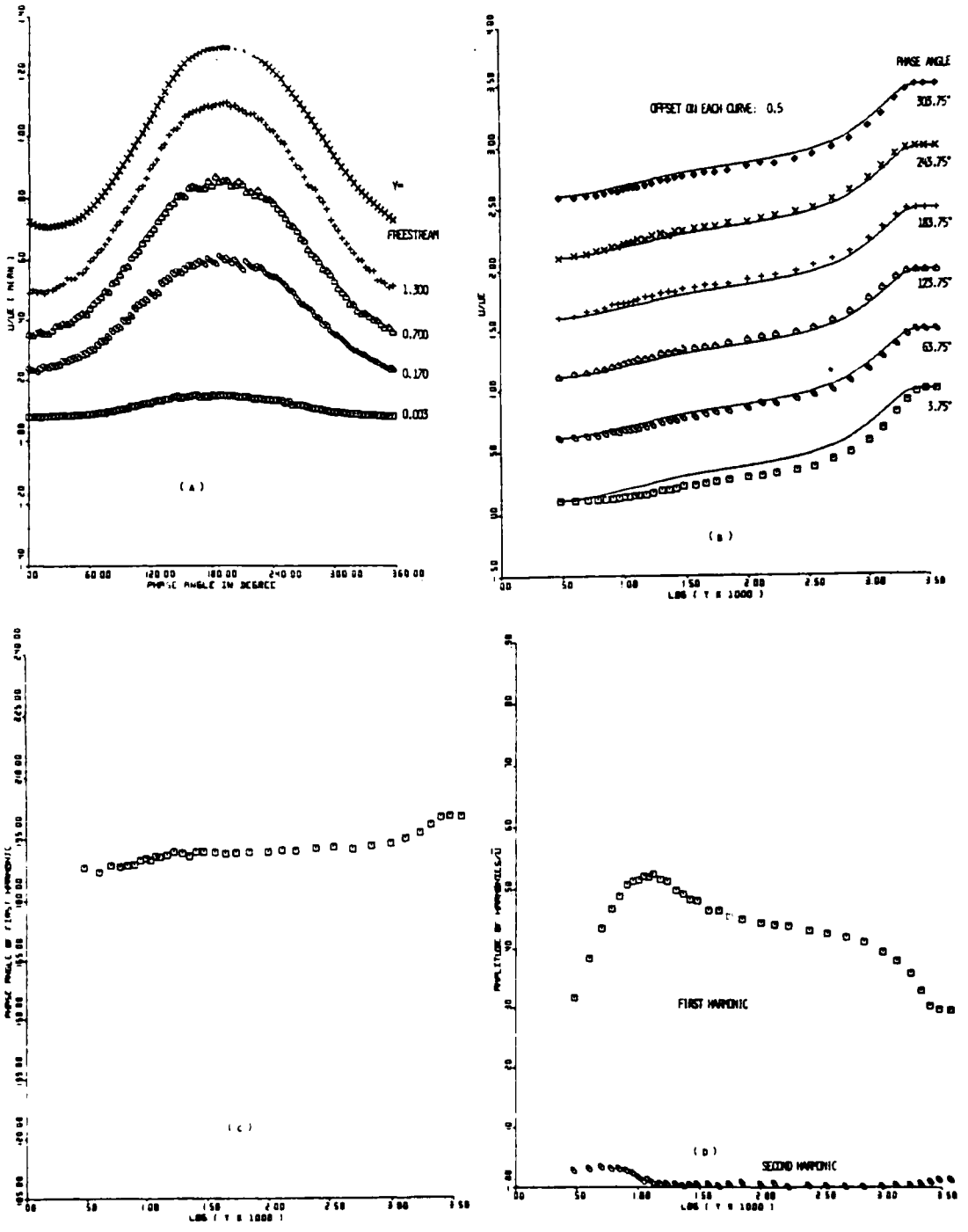

Figure 7. Flow A, ensemble-averaged normal hot-wire data, x=112 1/4 inches. Y in inches, base-10 logs; phase angle in degrees.

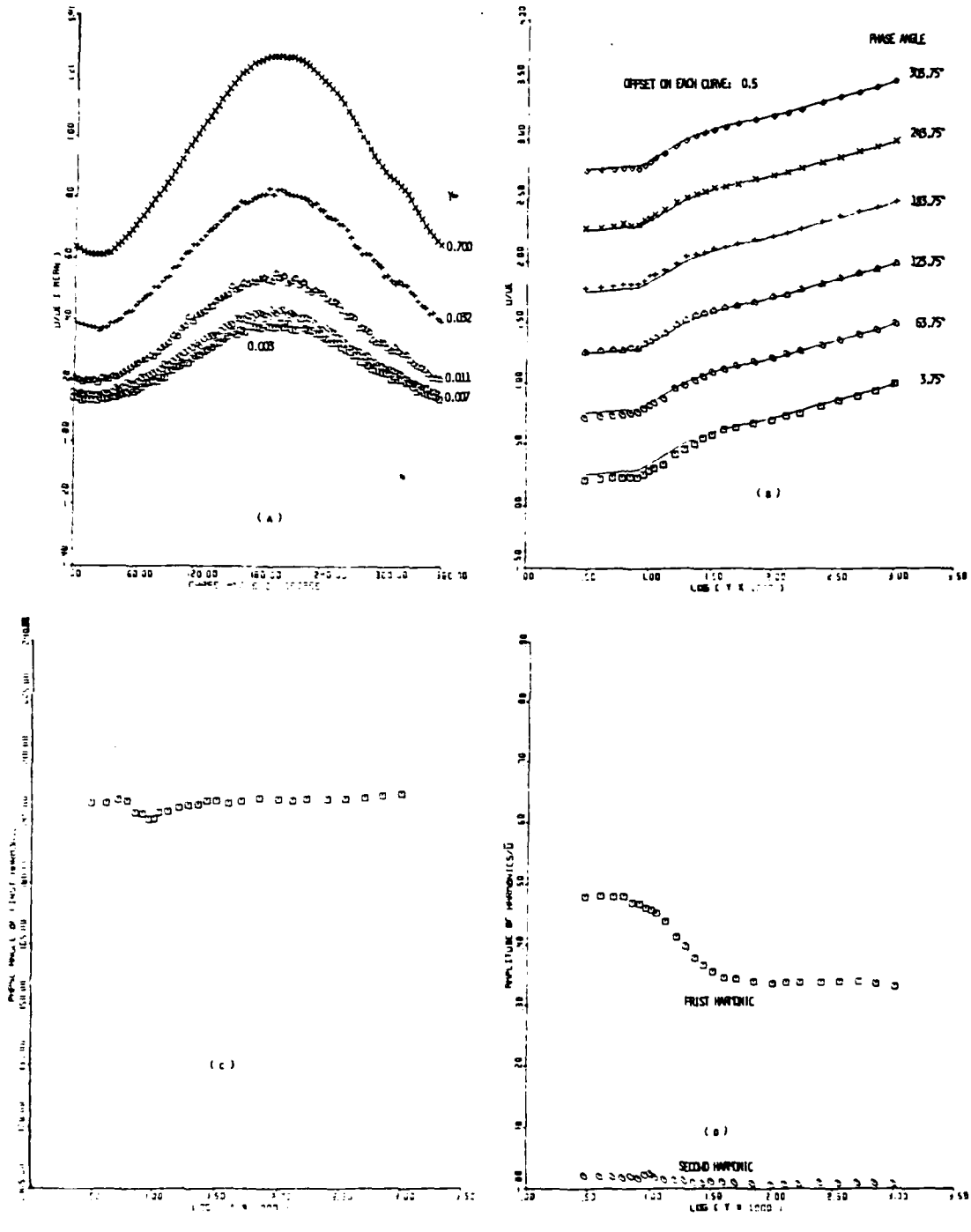

Figure 8. Flow B, ensemble-averaged normal hot-wire data, x= 52 1/2 inches. Y in inches, base-10 logs; phase angle in degrees.

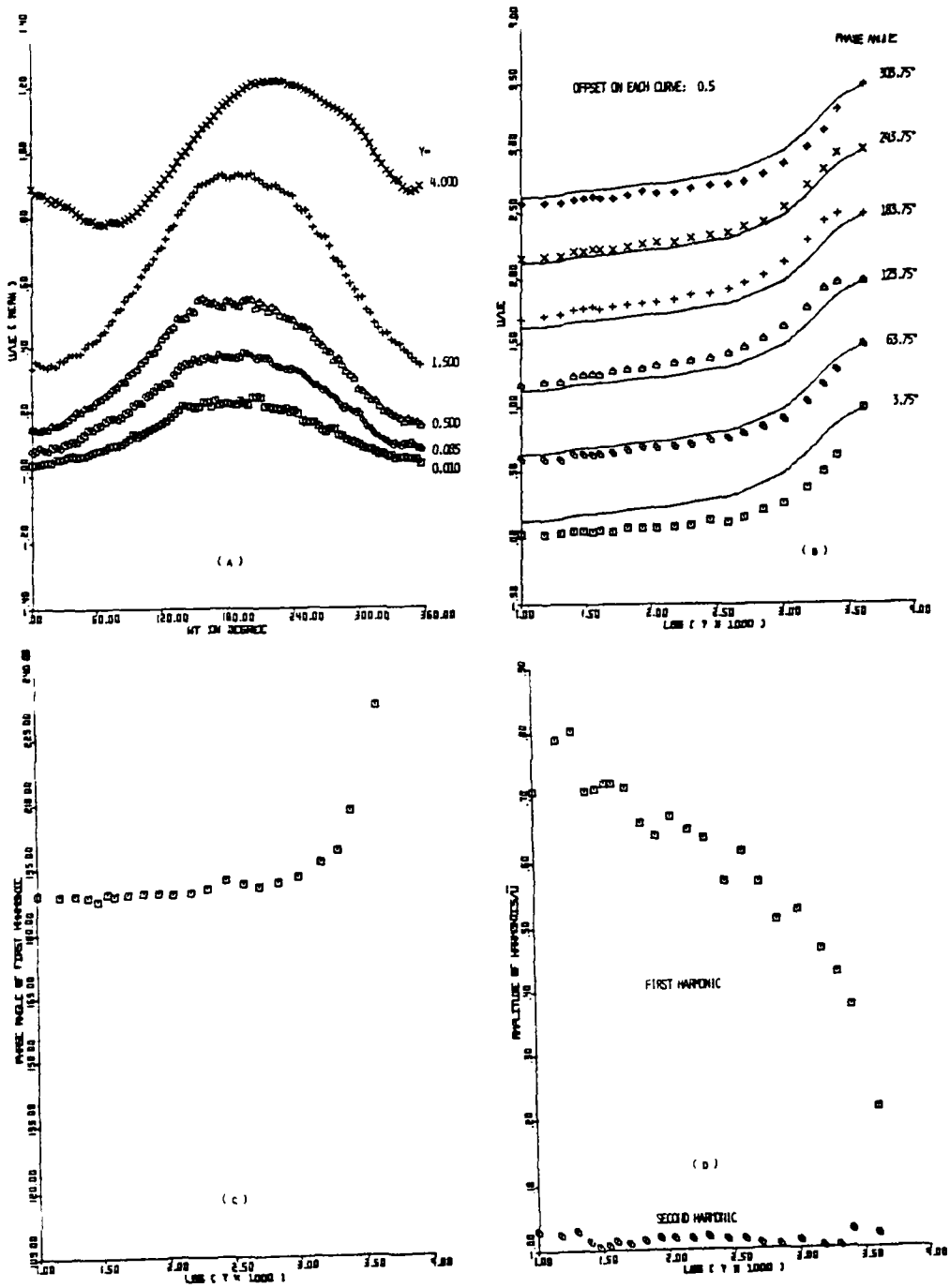

Figure 9. Flow A, ensemble-averaged laser anemometer data, x=120. Y in inches, base-10 logs; phase angle in degrees.

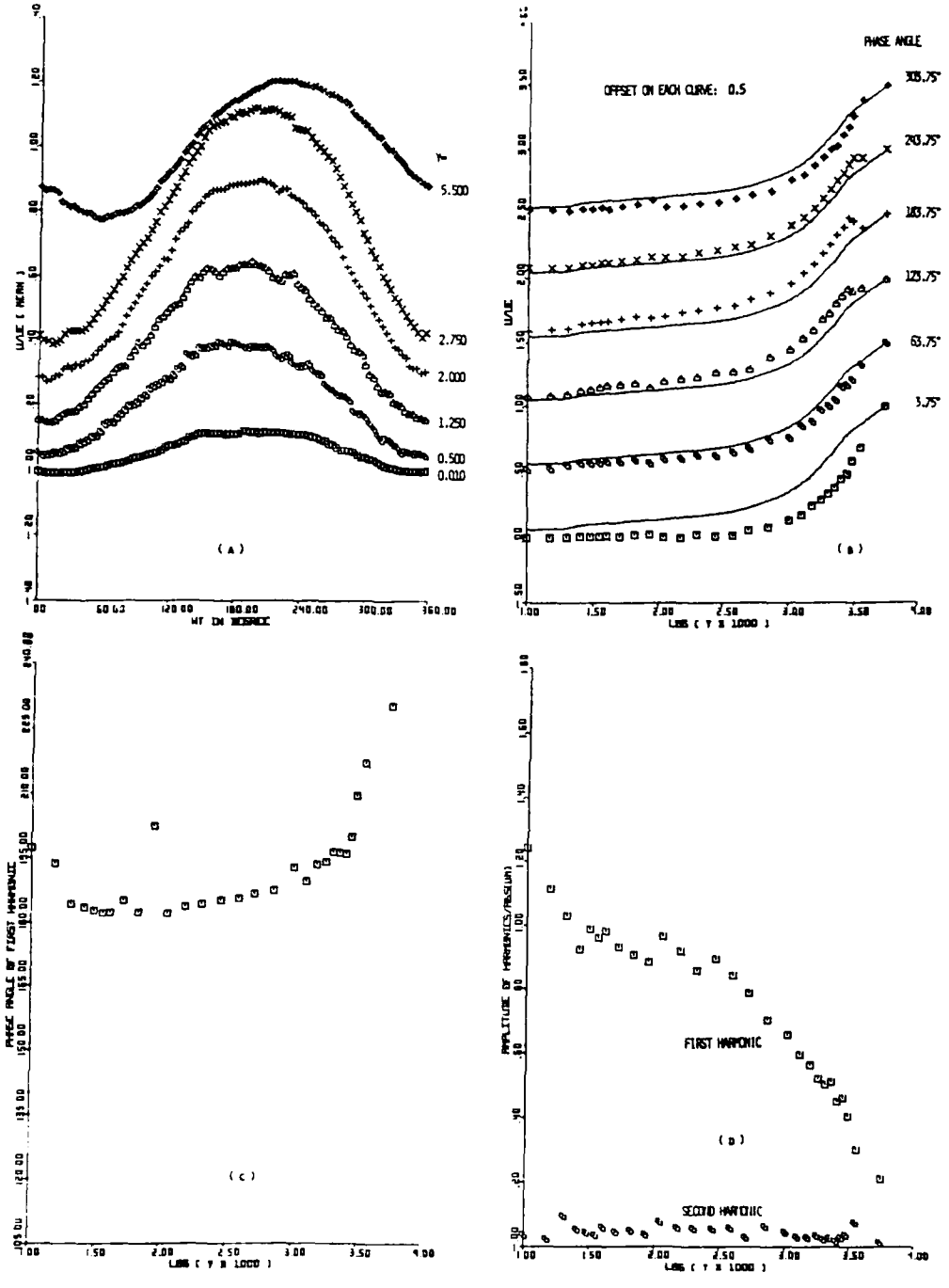

Figure 10. Flow A, ensemble-averaged laser anemometer data, x= 127 inches. Y in inches, base-10 logs; phase angle in degrees.

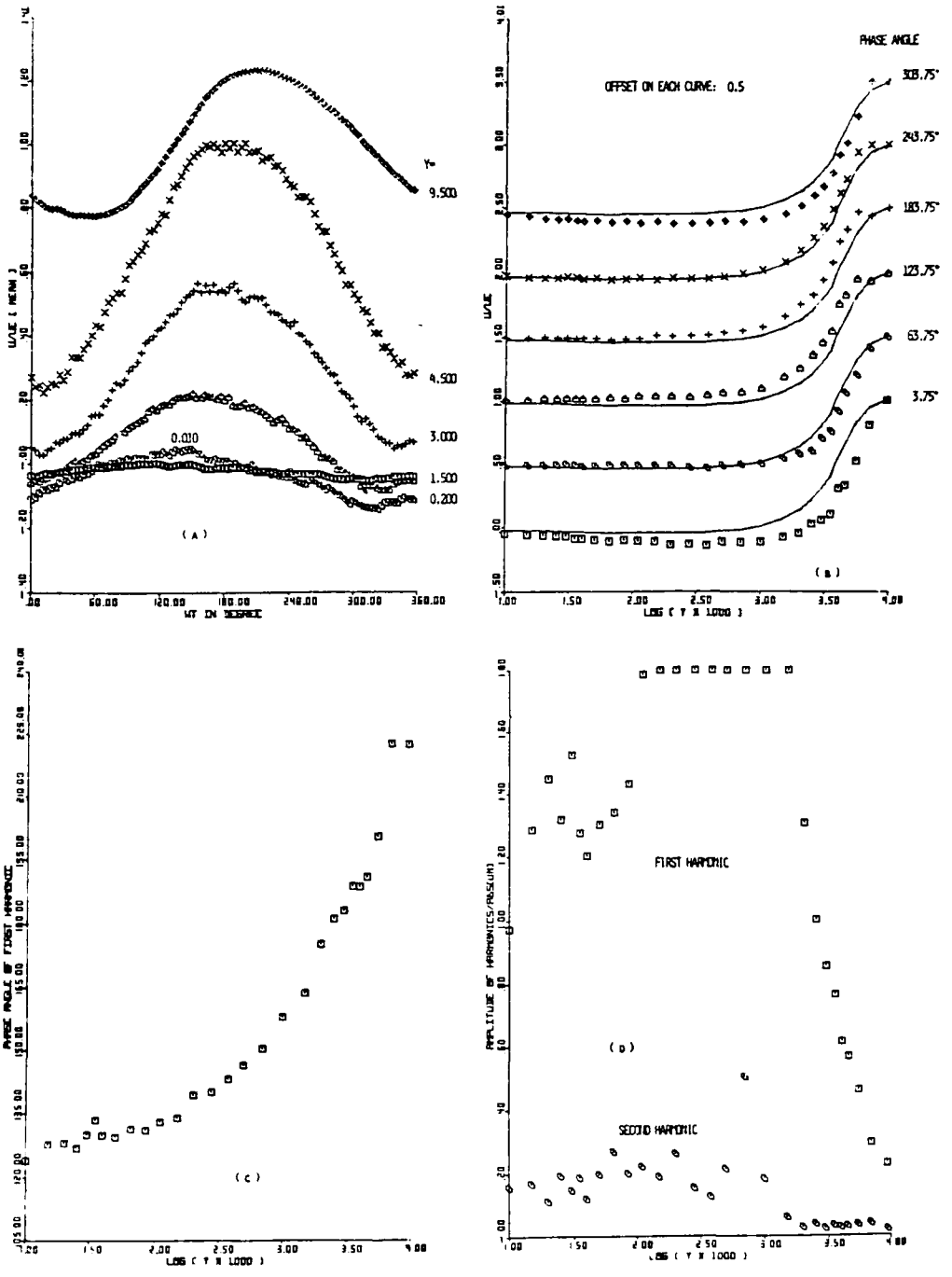

Figure 11. Flow A, ensemble-averaged laser anemometer data, x=144 inches. Y in inches, base-10 logs; phase angle in degrees.

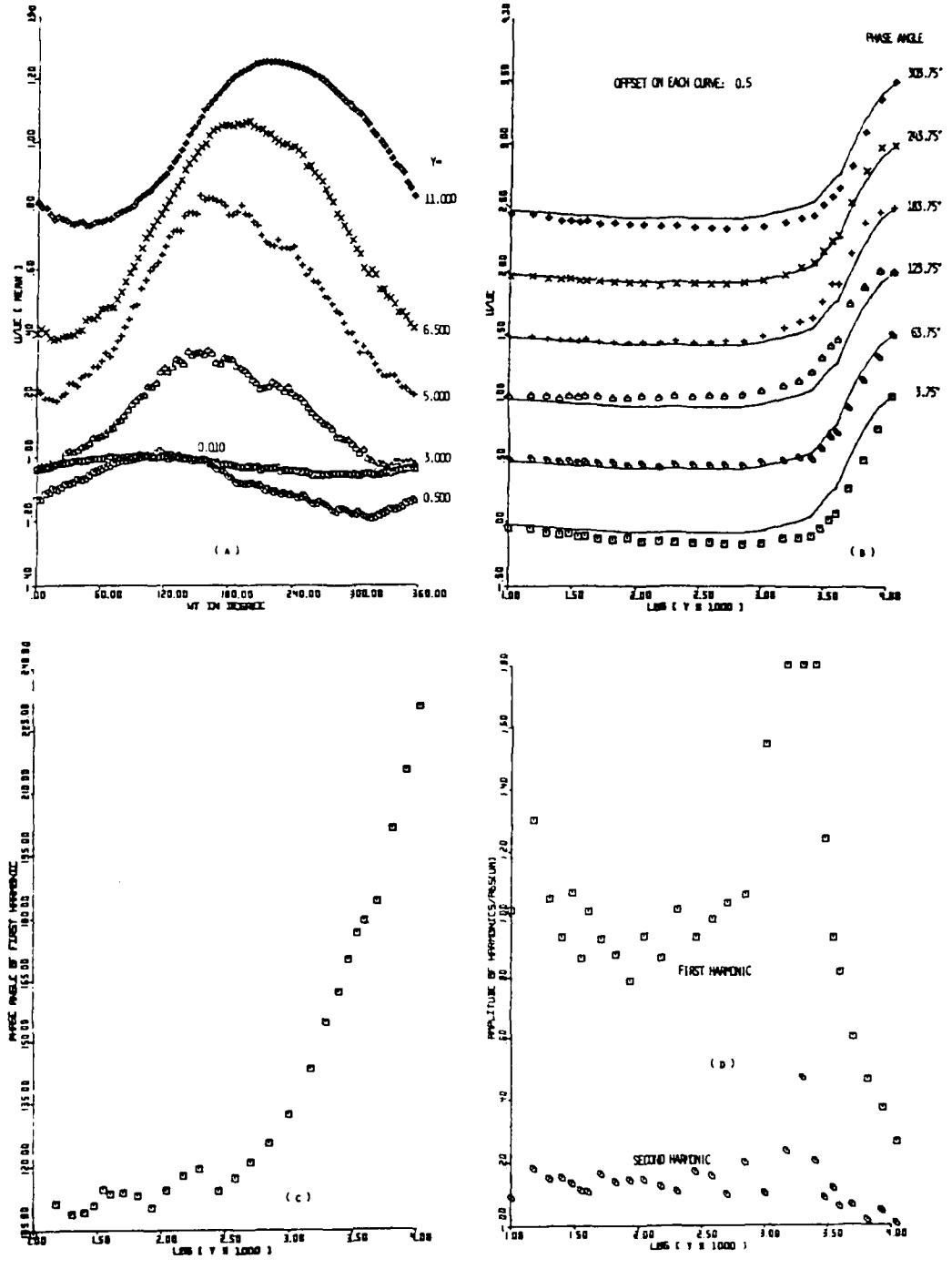

Figure 12. Flow A, ensemble-averaged laser anemometer data, x= 156 inches. base-10 logs; phase angle in degrees, Y in inches.

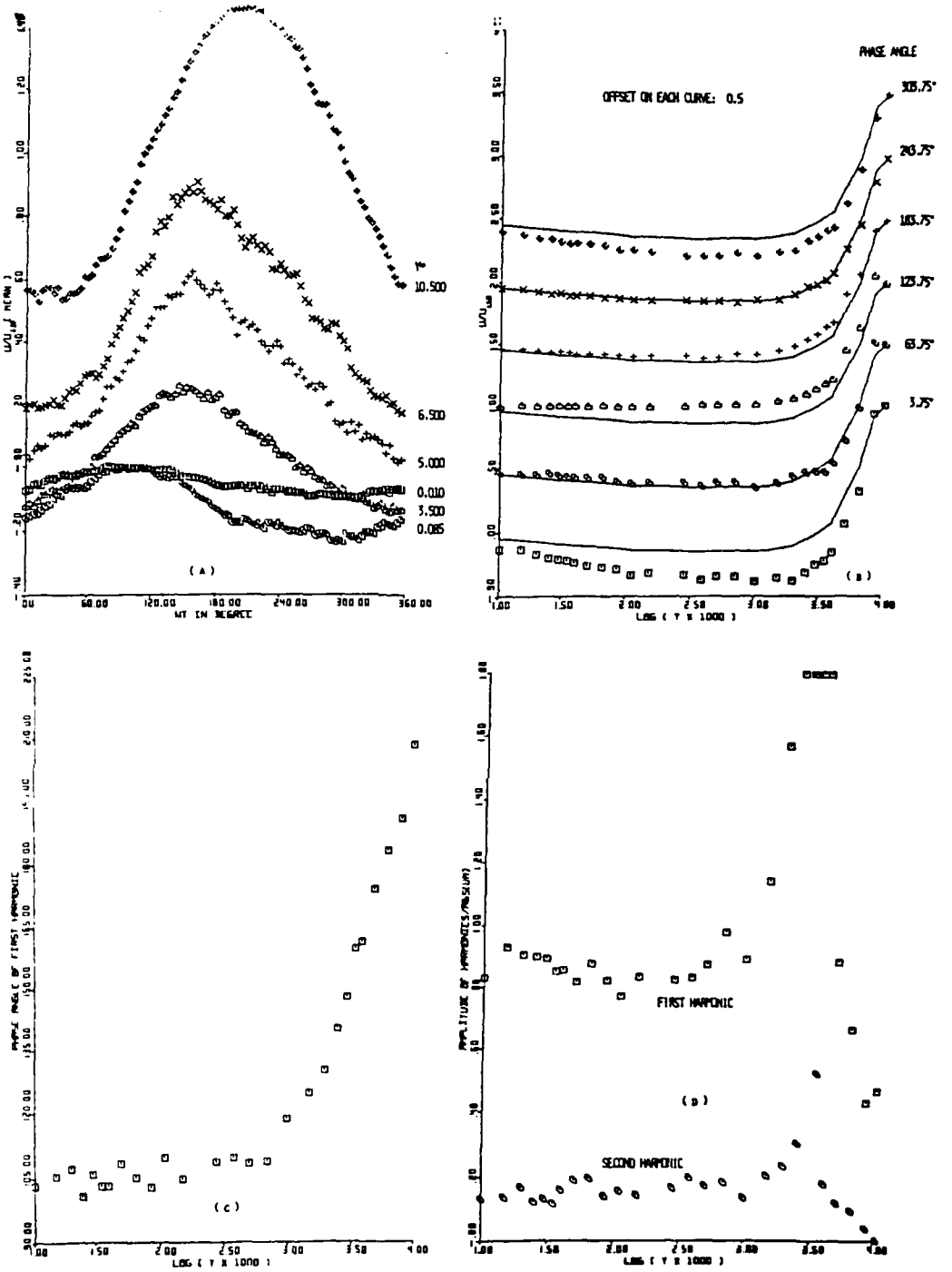

Figure 13. Flow A, ensemble-averaged laser anemometer data, x= 170 inches. Y in inches, base-10 logs; phase angle in degrees.

This leads us to believe that there is some sort of "critical layer." On the side of this critical layer nearer the wall the turbulence magnitude leads the periodic ensemble-averaged oscillatory velocity, while the ensemble-averaged oscillatory velocity leads the turbulence magnitude on the free-stream side of the critical layer, as shown in Figs. 14-17.

The amplitude of the first harmonic $U_1/\overline{U}$ is about constant in the logarithmic region and increases along the flow. The phase angle of the first harmonic U_1 is independent of y in the logarithmic region, as it must be when an inner wall layer and outer wake-like layer overlap (Simpson, 1977). Near separation (2.8 m) and downstream, increasingly larger phase leads of the entire logarithmic and backflow are observed (Fig. 7, 9-13).

Figures 14-17 show that the phase angles for the first harmonics of U, $\overline{u^2}$, $\overline{v^2}$, and $\overline{-uv}$ are nearly the same in the logarithmic region well upstream of separation. Near separation and downstream $\overline{-uv}$ and U appear to be in phase while $\overline{u^2}$ and $\overline{v^2}$ progressively lag $\overline{-uv}$ and U more in the downstream direction.

Figure 18 shows the friction factor for the time-averaged surface shearing stress for the flow with k = 0.55. These Cf/2 values are about 15% higher than those for the steady flow with the same time-averaged free-stream velocity. The surface element was calibrated in the steady flow just prior to the unsteady flow measurements, so the difference between the results from these two flows is distinct and not due to experimental uncertainties. Similar results were obtained for the k = 1.00 flow, but with the unsteady flow results being about 20% higher than for a comparable steady flow.

These higher mean skin friction results for the unsteady flows are believed to be at least partially due to first harmonic contributions to the mean dynamic pressure. In other words if the dynamic pressure is

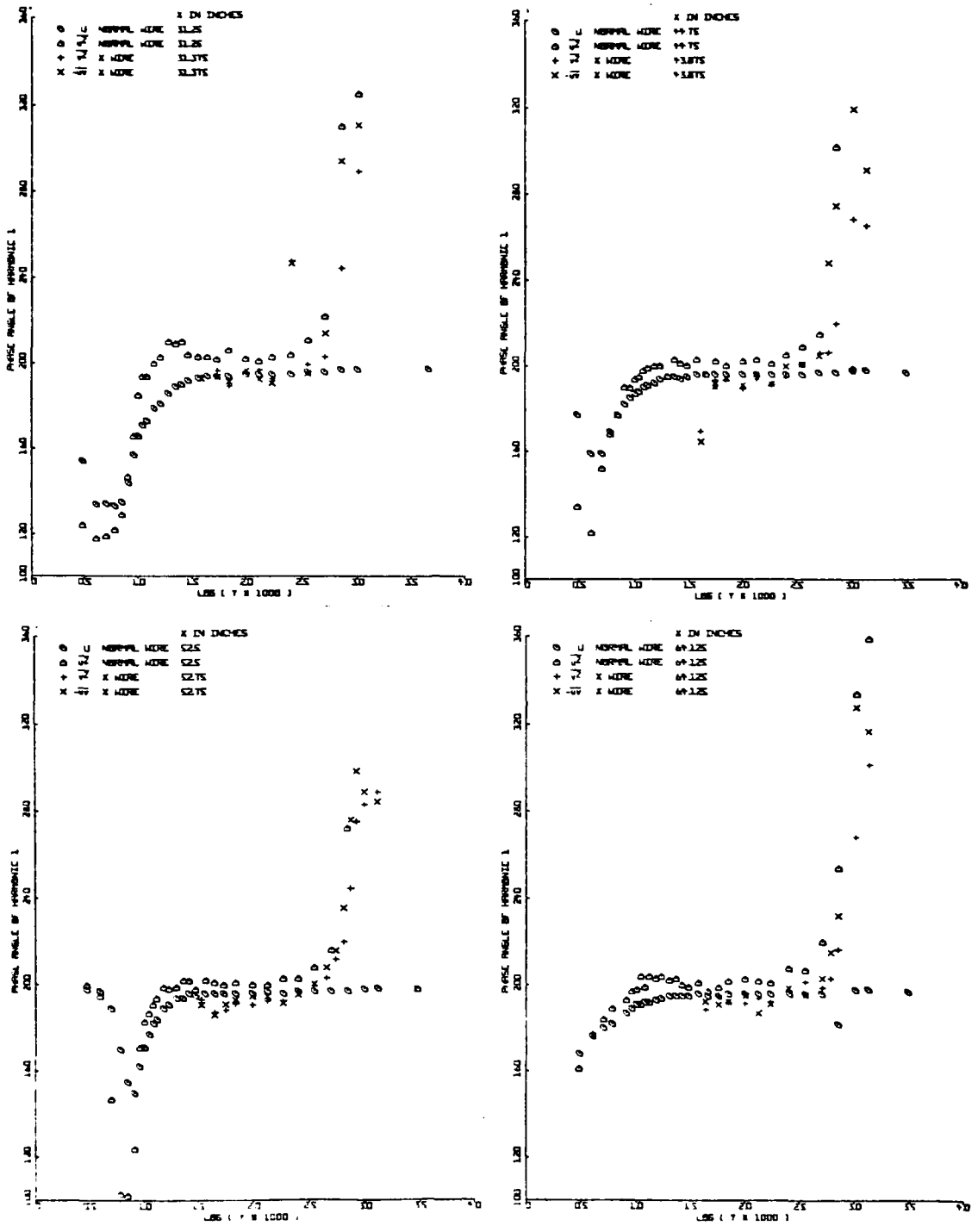

Figure 14. Phase angles of the first harmonics of U, $\overline{u^2}$, $\overline{v^2}$, and $-\overline{uv}$ at 31, 44, 52, and 64 inches.

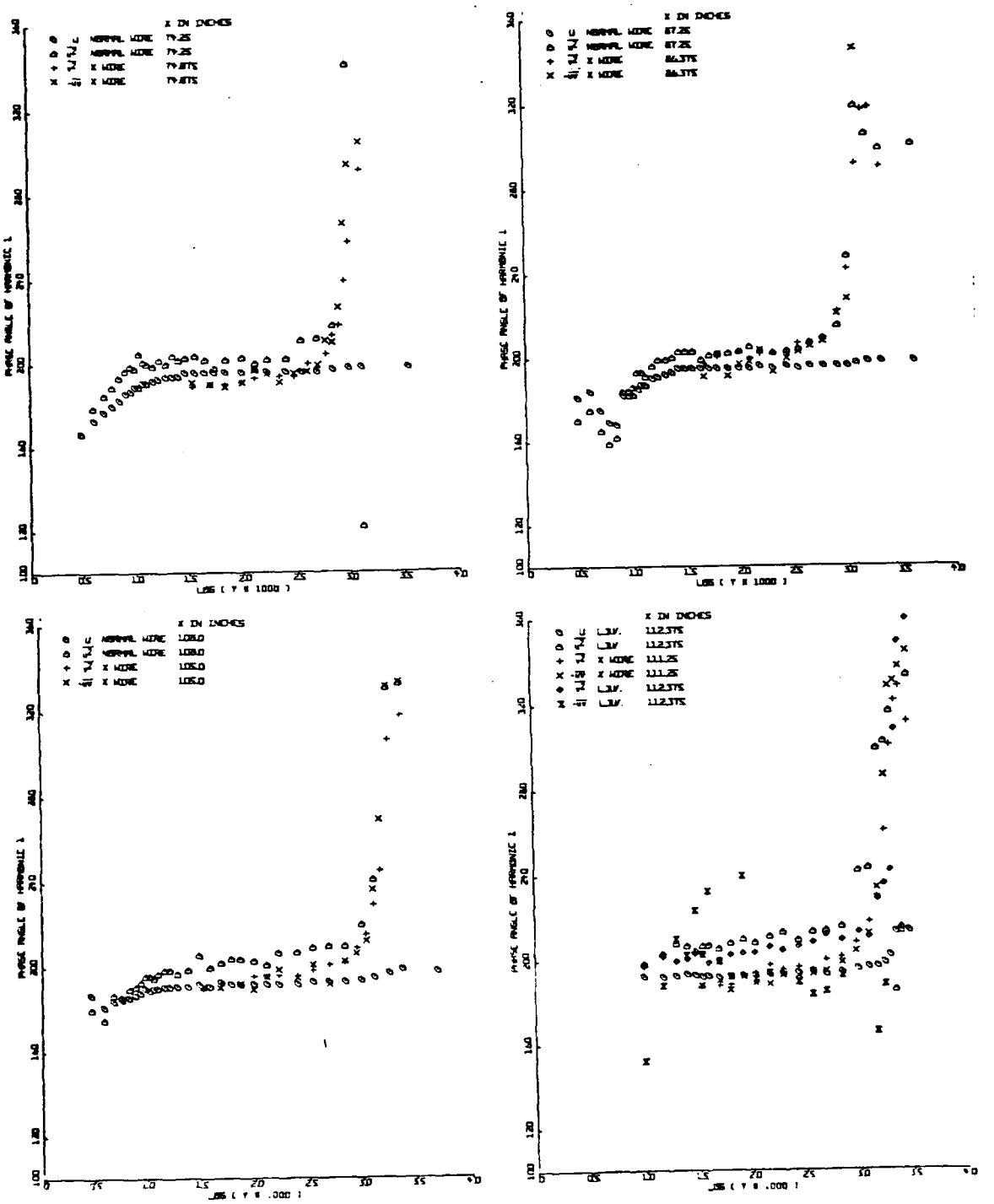

Figure 15. Phase angles of the first harmonics of U, $\overline{u^2}$, $\overline{v^2}$, and $\overline{-uv}$ at 74, 87, 105, 108, and 112 inches.

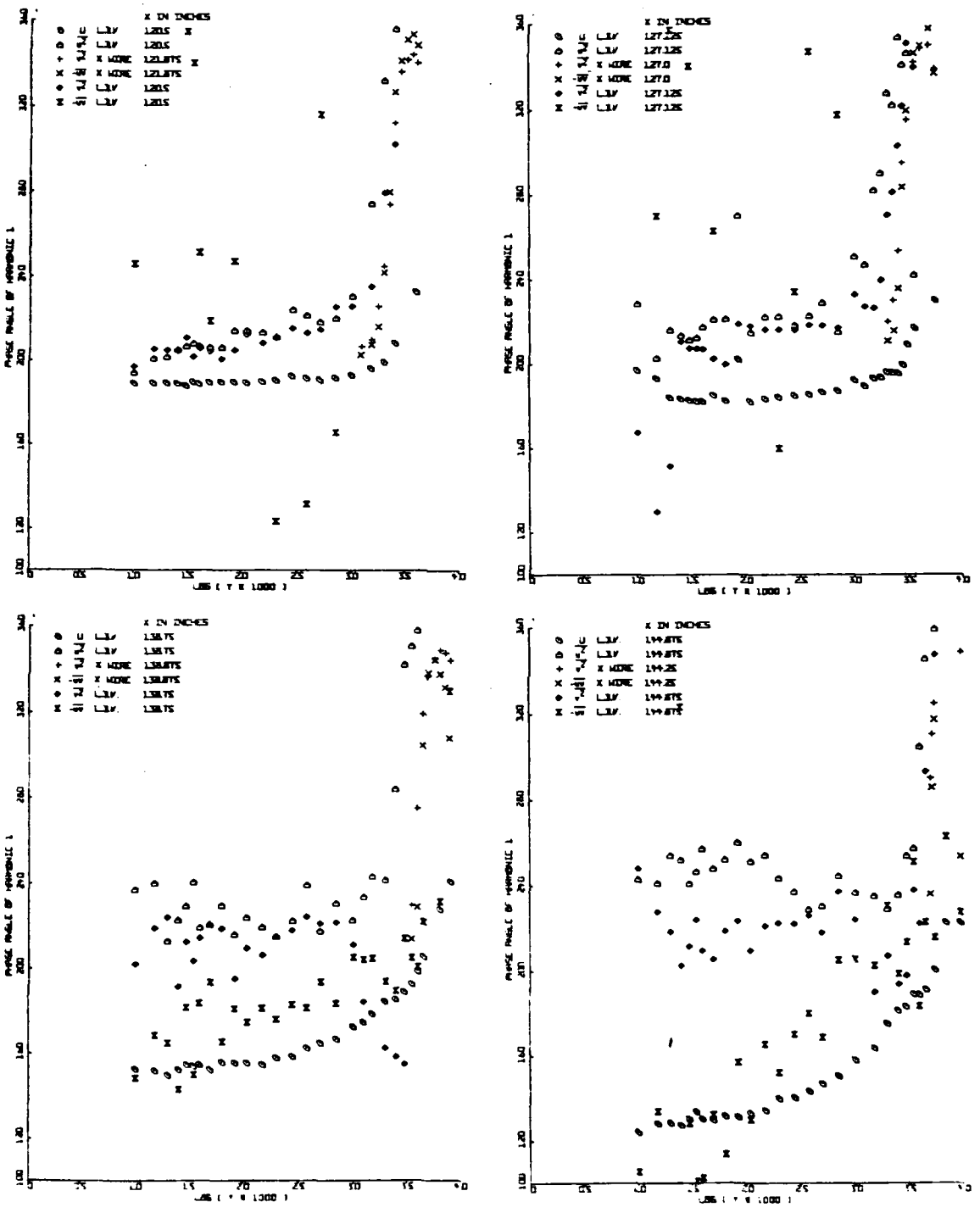

Figure 16. Phase angles of the first harmonics of U, $\overline{u^2}$, $\overline{v^2}$, and $-\overline{uv}$ at 121, 127, 138, and 144 inches.

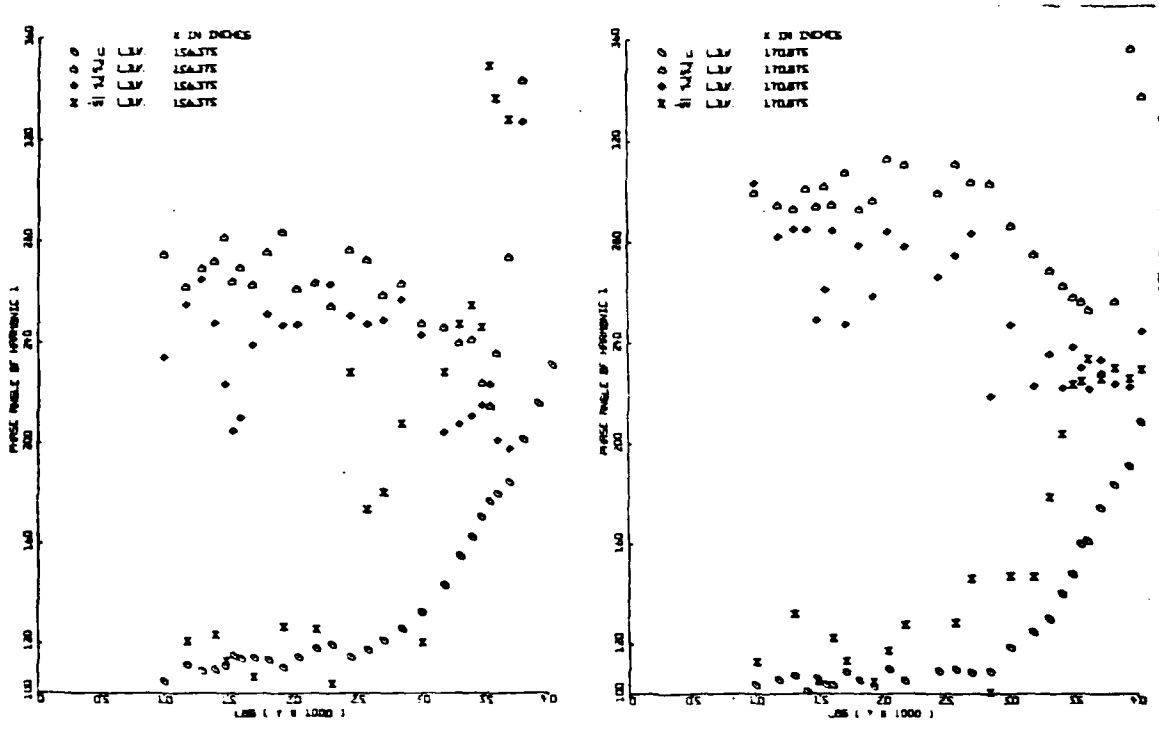

Figure 17. Phase angles of the first harmonics of U, $\overline{u^2}$, $\overline{v^2}$, and $-\overline{uv}$ at 156 and 171 inches.

$$\frac{\rho U_\infty^2}{2} = \frac{\rho}{2}\{\overline{U}_\infty + U_{\infty 1}\cos(\omega t - \Phi_1) + \ldots\}^2$$

$$= \frac{\rho \overline{U}_\infty^2}{2} + \frac{\rho U_{\infty 1}^2}{4} + \rho \overline{U}_\infty U_{\infty 1}\cos(\omega t - \Phi_1)$$

$$+ \text{higher harmonics}$$

then the second term on the right hand side arises due to the squared velocity. This term is only about 1/18 times the first term in these flows, so this effect alone cannot explain the increased mean shear stress.

Figure 18 also shows predicted mean skin friction coefficients from the Ludwieg and Tillman (1950) equation, using the time-averaged shape factor H and momentum thickness Reynolds number. Patel (1978) indicated that this is an adequate mean skin-friction relation for low amplitude flow oscillations of the order of 10% of the mean flow. However, as shown on these figures, these predictions are lower than or about equal to the steady freestream results. This indicates that the Ludwieg and Tillman equation is not satisfactory for moderately large oscillation amplitudes.

Figures 4 and 5 show that the phase angle of the first harmonic shearing stress for the two flows leads and lags, respectively, the velocity in the logarithmic region by about 3° to 5°. In essence the phase angle for the shear at the wall is the same as the velocity in the logarithmic region. Thus, at first glance these results tend to indicate that the significant phase angle variation observed in the viscous sublayer may be due to probe interference effects.

However, the ratio of the amplitude of the first harmonic to the mean surface shear is about 0.66 and 0.5 for the two flows, respectively. This means that the amplitude of the first harmonic to the local mean velocity

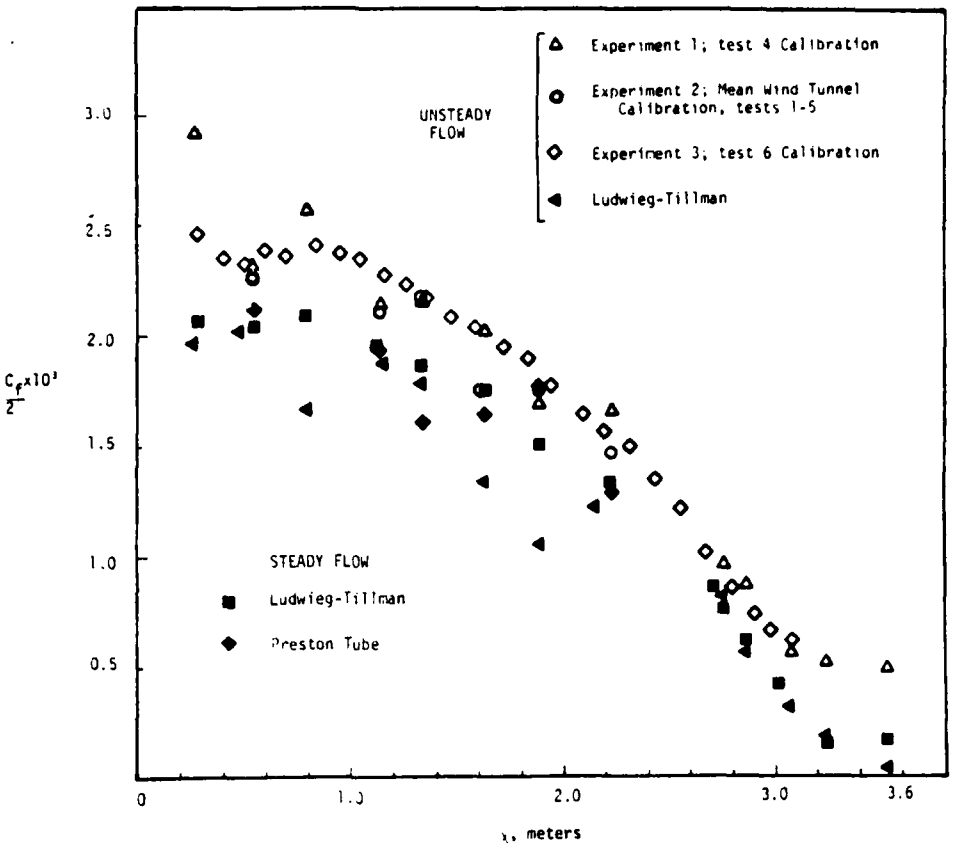

Figure 18. Time-averaged surface shearing stress for k = 0.55 unsteady flow and for steady flow with same freestream mean velocity distribution.

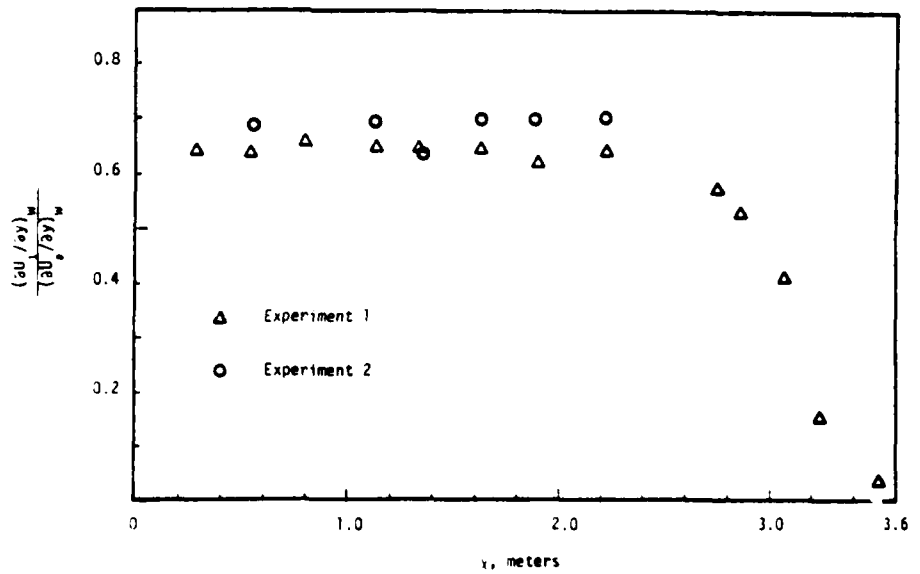

Figure 19. Amplitude of first harmonic to mean wall shearing stress, k = 0.55 flow.

must vary from 0.66 near the wall to lower values of the order of 1/3 in the logarithmic region for the k = 0.55 flow, as shown in Figures 6-8. The amplitude of the first harmonic shearing stress in the logarithmic region is also about 0.66 times the mean shearing stress and, is in phase with the first harmonic ensemble-averaged velocity in the logarithmic region. This is in agreement with the streamwise momentum equation for low reduced frequencies, which indicates that the total viscous and Reynolds shearing stress has the same phase angle through the near wall region. In fact these measurements confirm that the first harmonic wall shearing stress and the first harmonic velocity in the logarithmic region are in phase.

Using the momentum equation, the Reynolds shearing stress distribution near the wall was calculated from measured surface shearing stress and near wall velocity profiles. In all cases examined, the phase angle of the calculated first harmonic of the Reynolds shearing stress in the sublayer is less than that in the logarithmic region, a result which is similar to the phase lead shown in Figures 6(c), 7(c), and 8(c).

V. SUMMARY OF THE BEHAVIOR OF A SEPARATING UNSTEADY TURBULENT BOUNDARY LAYER

Here only the major conclusions about the nature of a separating unsteady turbulent boundary layer are discussed. A more complete description of the reasoning behind these conclusions is contained in Simpson et al. (1981).

Well upstream of separation the periodic frequency of the flow is much lower than the turbulence frequencies. Consequently there is little phase variation of U, $\overline{u^2}$, $\overline{v^2}$, and $\overline{-uv}$ in the outer part of the boundary layer. In the near wall region a substantial phase lead that cannot yet be explained is observed. There is some evidence mentioned in section IV above to support the possibility that this effect is real, rather than some rig dependent anomally. U, $\overline{u^2}$, $\overline{v^2}$, and $\overline{-uv}$ appear to be in phase in the logarithmic region.

The turbulence quantities $\overline{u^2}$, $\overline{v^2}$, and $\overline{-uv}$ are in phase in the outer region where the flow is intermittently turbulent and non-turbulent.

Near and beyond separation, the frequencies of the turbulence are much lower (Simpson et al., 1977), so that more interaction of the organized periodic and turbulent motions occurs. As pointed out in section IV above, there is increasing phase variation among U, $\overline{u^2}$, $\overline{v^2}$, and $\overline{-uv}$ in the separation region. After separation there is pressure gradient relief so that dP/dx is never negative. The amplitude of the freestream velocity oscillation becomes a smaller fraction of the local mean velocity. Eqn. (3.3) and Fig. 4 show that $d\phi_{1\infty}/dx \geq \omega/\overline{U}_E$ and that γ_{1E} approaches 180°, so that the pressure gradient dP/dx and the freestream velocity are almost in phase.

The law of the wall plots for the steady flow with the same mean streamwise velocity distribution (Simpson et al., 1980) indicate the existence of a logarithmic law, $U^+ = 5.62 \log y^+ + 5$, similar to the ones found by previous investigators. In conformity with the previous findings one can observe a gradually decreasing wake in the favourable pressure gradient region up to x = 1.33 m and a gradually increasing wake in the adverse pressure gradient region downstream of it. The mean unsteady flow also indicates the existence of the logarithmic region with a slope which is only slightly different (approximately 10%) but having an intercept almost the same as that for the steady flow. The behavior of the wake is also similar to that for the steady flow and very little differences are observed between the maximum wake defects for the two flows at the various streamwise locations. The unsteady flow at a lower Reynolds number is found to have approximately the same slope but a considerably different intercept as shown in Fig. 20.

This different slope and intercept for unsteady and steady flows cannot

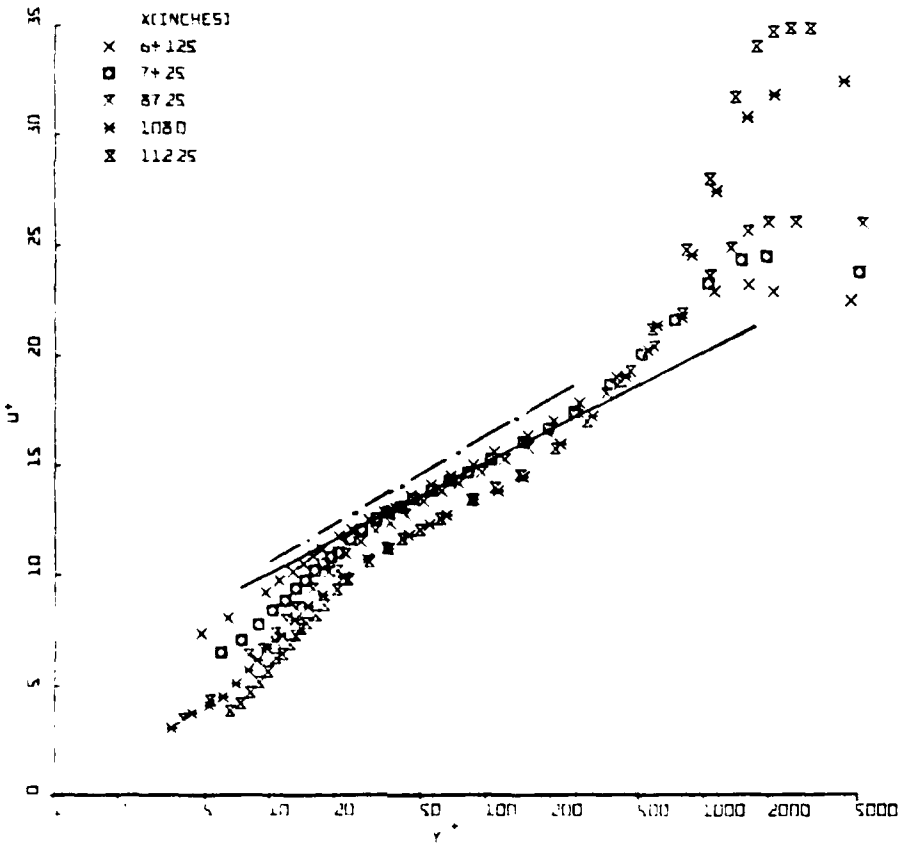

Figure 20. Mean velocity profiles of unsteady flow A in U^+ vs. log y^+ coordinates.

—— • —— $U^+ = 5.62 \log y^+ + 5.0$ steady flow.

———— $U^+ = 5.0 \log y^+ + 5.1$ for the three upstream unsteady flow stations.

be accounted for by the time-averaging process alone. In fact, by assuming that the logarithmic law of the wall for the steady flow holds for every phase of the unsteady flow and then time averaging the equation, it can be shown that the time-averaged slope decreases less than 3% while the intercept increases less than 3% from the steady flow equation. The much lower slope shown in Fig. 20 is mainly due to the higher measured mean skin friction values.

Just upstream of separation the mean velocity profiles closely obey Perry and Schofield's (1973) correlation of all types of adverse pressure gradient distribution boundary layers. This correlation requires that $(\overline{-uv})_{max}/\tau_w$ must exceed 1.5. Simpson et al. (1980) found that the mean velocity profiles for the same mean freestream velocity steady flow also obey this correlation.

Downstream of separation approximate mean velocity profile similarity is observed (Fig. 21) for the reverse flow region when the absolute value of the minimum mean velocity and the distance from the wall to its location are used as velocity and length scales. This profile shape is exactly the same as reported by Simpson et al. (1980) for the comparable steady freestream case even though the periodic ensemble-averaged velocity leads the freestream velocity oscillation by a large amount. As in the steady freestream velocity case, a law-of-the-wall profile based on the mean wall shear cannot hold since both U_N and N increase with streamwise distance, while the law-of-the-wall length scale ν/U_τ varies inversely with the velocity scale U_τ.

The turbulence structure is not greatly influenced by the unsteadiness upstream of separation. Eddy viscosity and mixing length distributions for the mean flow are closely the same as for the comparable steady freestream

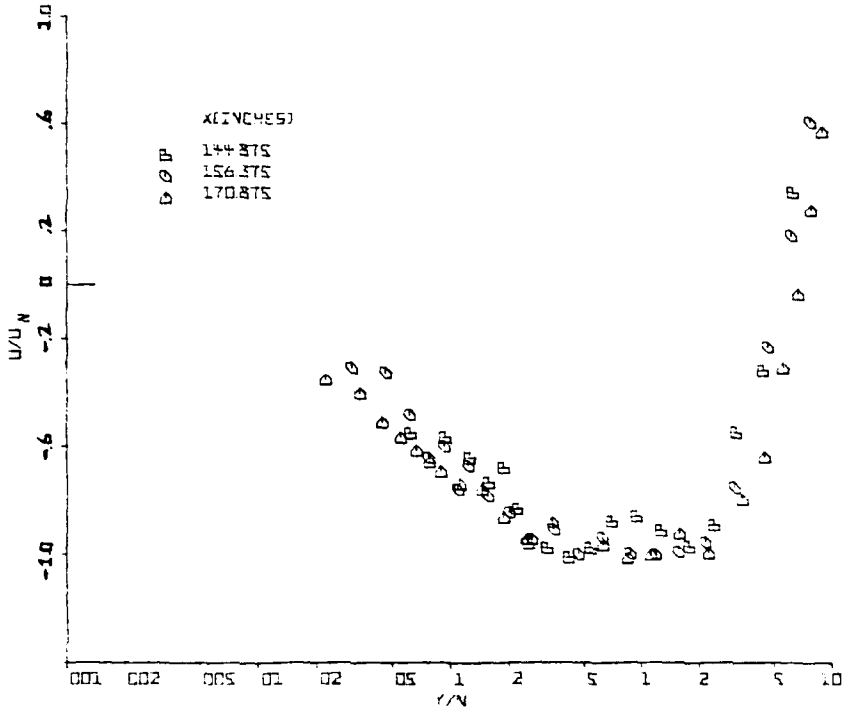

Figure 21. Normalized mean backflow velocity profiles for flow A: U_N and N, maximum mean backflow velocity and its distance from the wall, respectively.

flow. The eddy viscosity for the first harmonic is twice that of the mean flow, which is consistent with eqn. (1.6) and the fact that $(\overline{-uv})_1/(\overline{-uv})$ is twice $U_1/\bar{U}$ at a given location in the flow.

The Reynolds shearing stresses in the backflow region must be modeled by relating them to the turbulence structure and not to local mean velocity gradients, which is the same result for the comparable steady freestream case. The ensemble-averaged velocity profiles in the backflow are a result of ensemble-averaging the large turbulent fluctuations and are not related to the cause of the turbulence. Naturally, eddy viscosity and mixing length models are physically meaningless in the backflow, the eddy viscosity being negative and the mixing length being imaginary.

VI. FUTURE RESEARCH

As a result of the above observations, it is clear that several important newly observed phenomena are present in real unsteady turbulent boundary layers in practical axial compressors and turbines and helicopters. Insufficient measurements are currently available to quantitatively describe these phenomena over a range of reduced frequencies so further measurements are needed.

Since the periodic flow and the large-scaled outer region turbulence structure appear to interact more in the presence of unfavorable pressure gradients, some turbulence structure measurements such as the large eddy turbulence energy diffusion $\frac{\partial}{\partial y}(\overline{u^2v} + \overline{u^3})$ need to be made with the idea of relating their behavior to the phase variation of the several turbulence quantities in the boundary layer. This is being done for the current k = 0.55 flow under study.

The effect of oscillation waveform and amplitude on separation is being currently examined. A thermal tuft upstream-downstream intermittency probe has been developed for this research. Detailed LDV measurements of the separated zone are planned.

REFERENCES

Acharya, M. and Reynolds, W.C. 1975 "Measurements and Predictions of a Fully-Developed Turbulent Channel Flow with Imposed Controlled Oscillations," Rept. TF-8, Thermosciences Division, Dept. Mechanical Engineering, Stanford University.

Bellhouse, B.J. and Schultz, D.L., "Determination of Mean and Dynamic Skin Friction, Separation, and Transition in Low-Speed Flow with a Thin Film Heated Element," J. Fluid Mech., 24, pp. 379-400 (1966).

Benney, D.J. and Lin, C.C. 1960 "On the Secondary Motion Induced by Oscillations in a Shear Flow," Physics Fluids, 3, pp. 656-657.

Bowles, E.B. 1977 "Design, Construction, and Testing of Wall Jet-Wall Suction Boundary Layer Control System," Dept. of Civil/Mechanical Engrg. Internal Report WT-5, Southern Methodist University.

Bradshaw, P. 1978 "Structure of Turbulence in Complex Flows," paper 10, AGARD-LS-94.

Cousteix, J., Desopper, A., and Houdeville, R., "Structure and Development of a Turbulent Boundary Layer in an Oscillatory External Stream," Symposium on Turbulent Shear Flow, Pa. State Univ., April 18-20, 1977, paper 8-B.

Cousteix, J., Houdeville, R., and Raynaud, M. 1979 "Oscillating Turbulent Boundary Layer with a Strong Mean Pressure Gradient," Second Symposium on Turbulent Shear Flow, Imperial College, London, July 2-4, pp. 6.12-6.17.

Davis, R.E. 1974 "Perturbed Turbulent Flow, Eddy Viscosity and the Generation of Reynolds Stresses," J. Fluid Mech., 63, pp. 673-693.

Houdeville, R., Desopper, A., and Cousteix, J., "Analyse Experimentale des Caracteristiques d'une Couche Limite Turbulente en Ecoulement Pulse. Essai de Prevision Theorique," La Recherche Aerospatiale, Vol. 1976, No. 4, pp. 183-191.

Karlsson, S.K.F., "An Unsteady Turbulent Boundary Layer," J. Fluid Mech., 5, pp. 622-636, 1959.

Kenison, R.C., "An Experimental Study of the Effect of Oscillatory Flow on the Separation Region in a Turbulent Boundary Layer," paper 20, AGARD-CP-227 (1977).

Liepmann, H.W. and Skinner, G.T., "Shearing-stress Measurements by Use of a Heated Element," NACA TN 3268 (1954).

Ludwieg, H. and Tillman, W., "Investigations of the Wall-shearing Stress in Turbulent Boundary Layers," NACA TM 1285 (1950).

Miller, J.A., "A Simple Linearized Hot-Wire Anemometer," Journal of Fluids Engineering, Trans. ASME, Series I, Vol. 98, no. 3, pp. 550-557 (1976).

Murthy, V.W. and Rose, W.C., "Wall Shear Stress Measurements in a Shock-wave Boundary-layer Interaction," AIAA J., 16, pp. 667-672 (1978).

Patel, M.H., "On Turbulent Boundary Layers in Oscillatory Flow," Proc. R. Soc. London A, 353, pp. 121-144 (1977).

Patel, M.H., "Two Simplified Integral Approaches to Oscillating Turbulent Boundary Layers," Eurovisc, 1978; also Unpublished report, Dept. Mechanical Engineering, Univ. College, London.

Perry, A.E. and Schofield, W.H. 1973 "Mean Velocity and Shear Stress Distribution in Turbulent Boundary Layers," Physics Fluids, 16, pp. 2068-2074.

Rubesin, M.W., Okuno, A.F., Mateer, G.G., and Brosh, A. 1975 "A Hot-Wire Surface Gage for Skin Friction and Separation Detection Measurements," NASA TM X-62, 465.

Simpson, R.L., "Features of Unsteady Turbulent Boundary Layers as Revealed from Experiments," paper 19, Symposium on Unsteady Aerodynamics, NATO-AGARD, Ottawa, Canada, Sept. 1977; AGARD-CP-227.

Simpson, R.L. and Barr, P.W. 1975 "Laser Doppler Velocimeter Signal Processing Using Sampling Spectrum Analysis," Rev. Sci. Inst., 46, pp. 835-837.

Simpson, R.L. and Chew, Y.-T. 1979 "Measurements in Highly Turbulent Flows: Steady and Unsteady Separated Turbulent Boundary Layers," Proceedings of Third Int. Workshop on Laser Velocimetry, pp. 179-196, Hemisphere.

Simpson, R.L., Chew, Y.-T. and Shivaprasad, B.G., "Measurements of a Separating Turbulent Boundary Layer," Project SQUID Report SMU-4-PU, Purdue University, in press, 1980.

Simpson, R.L., Heizer, K.W., and Nasburg, R.E. 1979 "Performance Characteristics of a Simple Linearized Hot-Wire Anemometer," J. Fluids Engineering, 101, pp. 381-382.

Simpson, R.L., Sallas, J.J., and Nasburg, R.E. 1978 "Tailoring the Waveform of a Periodic Flow with a Programmable Damper," J. Fluids Engineering, 100, pp. 287-290.

Simpson, R.L., and Shackleton, C.R., "Laminariscent Turbulent Boundary Layers: Experiments on Nozzle Flows," Project SQUID Report SMU-2-PU (1977).

Simpson, R.L., Strickland, J.H., and Barr, P.W., "Features of a Separating Turbulent Boundary Layer in the Vicinity of Separation," J. Fluid Mech., 79, pp. 553-594 (1977).

Simpson, R.L. and Wallace, D.B., "Laminariscent Turbulent Boundary Layers: Experiments on Sink Flows," Project SQUID Report SMU-1-PU, (1975).

Telionis, D.P. 1977 "Unsteady Boundary Layers, Separated and Attached," paper 16, AGARD-CP-227.

Wood, N.B. 1975 "A Method for Determination and Control of the Frequency Response of the Constant-Temperature Hot-Wire Anemometer," J. Fluid Mech., 67, pp. 769-786.

APPENDIX A - SCIENTIFIC PERSONNEL SUPPORTED AND DEGREES AWARDED

Professor R. L. Simpson, Principal Investigator

Dr. Y.-T. Chew, Visiting Assistant Professor

Dr. B. G. Shivaprasad, Visiting Assistant Professor

Mr. C. R. Shackleton, MSME awarded Dec. 1976

Mr. E. Bowles, MSME awarded Dec. 1977

Mr. G. P. Kokolis, MSME awarded Dec. 1978

APPENDIX B - LIST OF PAPERS

1. Simpson, R.L. 1977 "Features of Unsteady Turbulent Boundary Layers as Revealed from Experiments," paper 19, Symposium on Unsteady Aerodynamics, NATO-AGARD, Ottawa, Canada, Sept. 1977; AGARD-CP-227.

2. Simpson, R.L., Sallas, J.J., and Nasburg, R.E. 1978 "Tailoring the Waveform of a Periodic Flow with a Programmable Damper," J. Fluids Engineering, *100*, pp. 287-290.

3. Simpson, R.L., Heizer, K.W., and Nasburg, R.E. 1979 "Performance Characteristics of a Simple Linearized Hot-Wire Anemometer," J. Fluids Engineering, 101, pp. 381-382.

4. Simpson, R.L. and Chew, Y.-T. 1979 "Measurements in Highly Turbulent Flows: Steady and Unsteady Separated Turbulent Boundary Layers," Proceeding of Third International Workshop on Laser Velocimetry, pp. 179-196, Hemisphere Press.

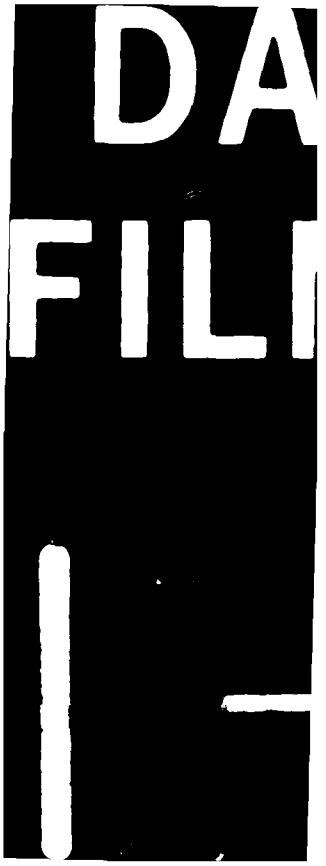
DA
FIL